

# Way to crosscheck $\mu - e$ conversion in the case of no signals of $\mu \rightarrow e\gamma$ and $\mu \rightarrow 3e$

Joe Sato<sup>1,\*</sup> and Masato Yamanaka<sup>2,†</sup><sup>1</sup>*Department of Physics, Saitama University, Shimo-okubo, Sakura-ku, Saitama 338-8570, Japan*<sup>2</sup>*Department of Physics, Nagoya University, Nagoya 464-8602, Japan*

(Received 16 January 2015; published 18 March 2015)

We consider the case that the  $\mu - e$  conversion signal is discovered but other charged lepton flavor violating (cLFV) processes will never be found. In such a case, we need other approaches to confirm the  $\mu - e$  conversion and its underlying physics without conventional cLFV searches. We study  $R$ -parity violating (RPV) SUSY models as a benchmark. We briefly review that our interesting case is realized in RPV SUSY models with reasonable settings in light of current theoretical and experimental status. We focus on the exotic collider signatures at the LHC ( $pp \rightarrow \mu^- e^+$  and  $pp \rightarrow jj$ ) as the other approaches. We show the correlations between the branching ratio of the  $\mu - e$  conversion process and cross sections of these processes. It is the first time that these correlations have been graphically shown. We exhibit the RPV parameter dependence of the branching ratio and the cross sections and discuss the feasibility of determining the parameters.

DOI: [10.1103/PhysRevD.91.055018](https://doi.org/10.1103/PhysRevD.91.055018)

PACS numbers: 12.60.-i, 12.60.Jv

## I. INTRODUCTION

Lepton flavor violation (LFV) is the clearest signal for physics beyond the Standard Model (SM) as it conserves lepton flavor exactly [1]. Therefore, extensive searches for LFV have been made since the muon was found. There have been searches for  $\mu \rightarrow e\gamma$  [2,3],  $\mu - e$  conversion [4], and  $\mu \rightarrow 3e$  [5]. In all of these processes, both the muon and electron number are violated. There are also LFV searches with the tau lepton [6–9]. Despite much effort, we have not found any LFV signals with charged leptons. LFV had, however, been found in neutrino oscillation [10,11], and it indeed requires us to extend the SM so that physics beyond the SM must include LFV. This fact also gives us a strong motivation to search for charged lepton flavor violation (cLFV). Indeed, the MEG Collaboration has tried to observe the process  $\mu \rightarrow e\gamma$  and provided a significant upper bound on its branching ratio [3]. Another effort at the LHC gave some of the upper limits on tau number violation [12], though at this moment more stringent limits are given by the Belle Collaboration.

Along this line, new experiments to search for cLFV will start soon. COMET [13,14] and DeeMe [15] will launch within a few years and search  $\mu - e$  conversion. In these experiments, muons are trapped by a target nucleus (carbon, aluminum, titanium, and so on), then, if cLFV exists, they convert into electrons.

If COMET and DeeMe observe the conversion process, then with what kind of new physics should we interpret it? Now it is worth considering again since we are in between two kinds of cLFV experiments with muons.

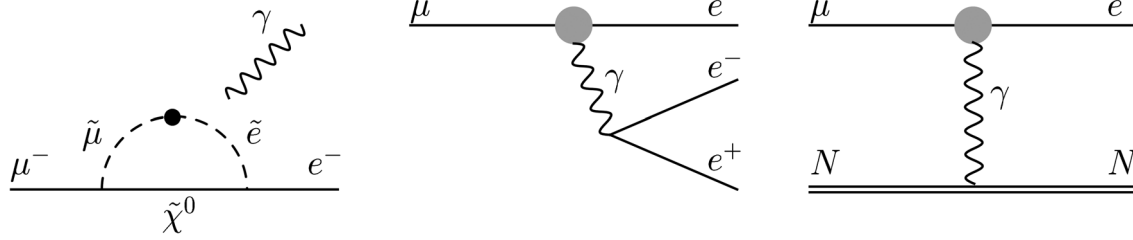
For several decades, theories with supersymmetric extension have been the most studied. These theories include a source of LFV. It is realized by the fact that the scalar partner of the charged leptons can have a different flavor basis from that of the charged leptons. In addition,  $R$  parity is often imposed on this class of the theory [16,17]. With it, the  $\mu \rightarrow e\gamma$  process has the largest branching ratio among the three cLFV processes. This occurs through the dipole process depicted in Fig. 1 and the other two,  $\mu - e$  conversion and  $\mu \rightarrow 3e$ , are realized by attaching a quark line and an electron line, respectively, at the end of the photon line, giving an  $O(\alpha)$  suppression. Those branching ratios must be smaller than that of  $\mu \rightarrow e\gamma$ . At this moment, however, the upper bounds for those branching ratios are almost the same as each other. It means if COMET and DeeMe observe a cLFV, which is the  $\mu - e$  conversion process, we have to discard this scenario.

It is, however, possible to find a theory easily in which COMET and DeeMe find cLFV first. To see this we first note that the  $\mu \rightarrow e\gamma$  process occurs only at loop level due to the gauge invariance, while the other two can occur as a tree process. Therefore, in this case, we have to consider a theory in which the  $\mu - e$  conversion process occurs as a tree process. In other words, we have to assume a particle which violates muon and electron number. Since  $\mu - e$  conversion occurs in a nucleus, it also couples with quarks with flavor conservation. Furthermore, it is better to assume that it does not couple with two electrons as we have not observed  $\mu \rightarrow 3e$ .

In this paper we consider the case that COMET and DeeMe indeed observe the cLFV process, while all the other experiments do not observe anything new. With this situation, we need to understand how to confirm the cLFV in other experiments. The way of the confirmation depends on a theory considered. Unfortunately, in this case, other

\*joe@phy.saitama-u.ac.jp

†yamanaka@eken.phys.nagoya-u.ac.jp

FIG. 1. cLFV processes in supersymmetric models with  $R$ -parity conservation.

new physics signals are expected to be quite few in number since the magnitude of the cLFV interaction is so small due to its tiny branching ratio. Therefore, it is very important to simulate now how to confirm the COMET and DeeMe signal and the new physics. As a benchmark case, we study a supersymmetric standard model without  $R$  parity [18]. In this kind of theory, the scalar lepton mediates  $\mu \leftrightarrow e$  flavor violation. The  $R$ -parity-violating (RPV) theory is strongly motivated also by the fact that we have not observed any typical SUSY signals.

Note that our aim in the study is not to put bounds on RPV couplings but to find a way of confirming “the muon conversion signal” when only the  $\mu - e$  conversion is found among the conventional cLFVs. We emphasize that it is the first time to consider the correlation among the branching ratio of the  $\mu - e$  conversion and other observables like the cross sections of  $pp \rightarrow \mu^- e^+$  and  $pp \rightarrow jj$  in RPV models when the  $\mu - e$  conversion signal is discovered but other cLFV process signals have not been found. There are, however, many studies on the bounds placed on RPV couplings from the  $\mu - e$  conversion [19–23].

This paper is organized as follows. First, in Sec. II, we sort out what kind of framework is expected in our interesting situation and what distinctive processes are expected to appear in the framework. Then we briefly review a theory with  $R$ -parity violation and show our setup. Next, in Sec. III we discuss what processes can signify the theory. In Sec. IV we give the results and discuss how to confirm the scenario depending on the parameters. Finally, we summarize our work in Sec. V.

## II. FRAMEWORK OF $\mu - e$ CONVERSION-DOMINANCE AND RPV SCENARIO AS THE BENCHMARK

Our interesting situation is that COMET and DeeMe observe the cLFV signal first. To realize the situation with minimal and simplest extension, we consider a massive mediator particle, which violates both muon and electron number and has the flavor-conserving couplings with quarks.<sup>1</sup> In this framework, other muon cLFV processes

<sup>1</sup>We have another possibility to build a framework in which  $\mu$ - $e$  conversion is dominant via loop processes [24–27]. In this work, however, we concentrate on the simplest framework wherein  $\mu - e$  conversion occurs at a tree process.

( $\mu \rightarrow e\gamma$ ,  $\mu \rightarrow 3e$ ,  $\mu^- e^- \rightarrow e^- e^-$  in muonic atom [28], and so on) occur at least at the two-loop level. At one glance, the massive mediator particle can connect with the photon via the quark loop shown in Fig. 2. The contribution of the loop of the diagram is proportional to

$$e \frac{m_q q_\mu}{8\pi^2} \int_0^1 dx (1-2x) \log(m_q^2 - (x-x^2)q^2) \propto q^2 q_\mu, \quad (1)$$

where  $q_\mu$  is the four-momentum of the photon. The contribution to cLFV, therefore, vanishes with the on-shell photon ( $q^2 = 0$ ) for  $\mu \rightarrow e\gamma$  and with the  $\bar{e}\gamma_\mu e$  attached for  $\mu \rightarrow 3e$  due to gauge symmetry ( $q^\mu \bar{e}\gamma_\mu e = 0$ ). Thus, these processes occur at the two-loop level. Furthermore, these loop processes are much further suppressed by higher-order couplings, gauge invariance, and so on. Therefore, we do not study these processes here.

In the simplest framework with the massive mediator particle, some characteristic signals inevitably appear, such as dijet and  $\mu^- e^+$  production with the  $s$ -channel massive mediator exchange at the LHC, muonium conversion  $\mu^+ e^- \rightarrow \mu^- e^+$ , and so on. These processes are key ingredients to confirm the  $\mu - e$  conversion signal and its underlying physics without conventional cLFV searches.

The simplest framework is naturally realized in  $R$ -parity-violating SUSY models. In general, the supersymmetric gauge-invariant superpotential contains the  $R$ -parity-violating terms [29–31],

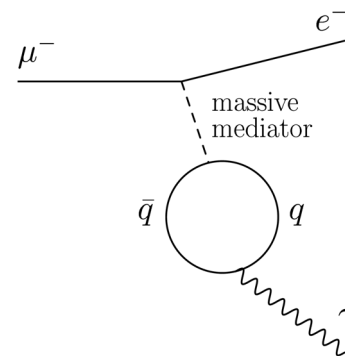


FIG. 2. Possible one-loop diagram for  $\mu \rightarrow e\gamma$ . It is, however, proportional to  $q^2 q^\mu$  and, hence, vanishes with the on-shell photon ( $q^2 = 0$ ) and with  $\bar{e}\gamma_\mu e$  attached due to gauge symmetry.

$$\mathcal{W}_{\text{RPV}} = \lambda_{ijk} L_i L_j E_k^c + \lambda'_{ijk} L_i Q_j D_k^c + \lambda''_{ijk} U_i^c D_j^c D_k^c, \quad (2)$$

where  $E_i^c$ ,  $U_i^c$ , and  $D_i^c$  are  $SU(2)_L$  singlet superfields, and  $L_i$  and  $Q_i$  are  $SU(2)_L$  doublet superfields. Indices  $i$ ,  $j$ , and  $k$  represent the generations. We take  $\lambda_{ijk} = -\lambda_{jik}$  and  $\lambda''_{ijk} = -\lambda''_{ikj}$ . The first two terms include lepton number violation, and the last term includes baryon number violation. Since some combinations of these terms accelerate proton decay, we omit the last term. Thus the RPV processes are described by the following Lagrangian:

$$\begin{aligned} \mathcal{L}_{\text{RPV}} &= \mathcal{L}_\lambda + \mathcal{L}_{\lambda'}, \\ \mathcal{L}_\lambda &= \lambda_{ijk} [\tilde{\nu}_{iL} \bar{e}_{kR} e_{jL} + \tilde{e}_{jL} \bar{e}_{kR} \nu_{iL} + \tilde{e}_{kR}^* \overline{(\nu_{iL})^c} e_{jL} - (i \leftrightarrow j)] \\ &\quad + \text{H.c.}, \\ \mathcal{L}_{\lambda'} &= \lambda'_{ijk} [\tilde{\nu}_{iL} \bar{d}_{kR} d_{jL} + \tilde{d}_{jL} \bar{d}_{kR} \nu_{iL} + \tilde{d}_{kR}^* \overline{(\nu_{iL})^c} d_{jL} \\ &\quad - \tilde{e}_{iL} \bar{d}_{kR} u_{jL} - \tilde{u}_{jL} \bar{d}_{kR} e_{iL} - \tilde{d}_{kR}^* \overline{(e_{iL})^c} u_{jL}] + \text{H.c.} \end{aligned} \quad (3)$$

Our interesting situation is that only  $\mu - e$  conversion is discovered, and other cLFV processes are never observed. The situation is realized under the following three conditions set on the RPV interaction:

- (1) Only the third-generation slepton contributes to the RPV interactions.
- (2) For quarks, flavor diagonal components are much larger than off-diagonal components, i.e., CKM-like matrix,  $\lambda'_{ijj} \gg \lambda'_{ijk} (j \neq k)$ .
- (3) The generation between left-handed and right-handed leptons is different,  $\lambda_{ijk} (i \neq k \text{ and } j \neq k)$ .

Condition 1 is naturally realized by the RG-evolved SUSY spectrum with universal soft masses at the GUT scale. For simplicity, we decouple other SUSY particles except for the third-generation sleptons. Condition 2 is also obtained in most cases unless we introduce additional sources of flavor violations. Condition 3 is artificially introduced to realize the interesting situation in this work—that COMET finds the cLFV process, while all the other experiments fail to observe anything new at the same time (see Introduction). Under these conditions, the general Lagrangian (3) is reduced as follows:

$$\begin{aligned} \mathcal{L}_{\text{RPV}} &= \mathcal{L}_\lambda + \mathcal{L}_{\lambda'}, \\ \mathcal{L}_\lambda &= 2[\lambda_{312} \tilde{\nu}_{\tau L} \bar{\mu} P_L e + \lambda_{321} \tilde{\nu}_{\tau L} \bar{e} P_L \mu + \lambda_{132} \tilde{\tau}_L \bar{\mu} P_L \nu_e + \lambda_{231} \tilde{\tau}_L \bar{e} P_L \nu_\mu \\ &\quad + \lambda_{123} \tilde{\tau}_R^* \overline{(\nu_{eL})^c} P_L \mu + \lambda_{213} \tilde{\tau}_R^* \overline{(\nu_{\mu L})^c} P_L e] + \text{h.c.}, \\ \mathcal{L}_{\lambda'} &= [\lambda'_{311} (\tilde{\nu}_{\tau L} \bar{d} P_L d - \tilde{\tau}_L \bar{d} P_L u) + \lambda'_{322} (\tilde{\nu}_{\tau L} \bar{s} P_L s - \tilde{\tau}_L \bar{s} P_L c)] + \text{H.c.} \end{aligned} \quad (4)$$

Processes described by the Lagrangian (4) strongly depends on the values of  $\lambda'_{311}$  and  $\lambda'_{322}$ . In this work, we study three cases:

- case-I  $\lambda'_{311} \neq 0$  and  $\lambda'_{322} = 0$
- case-II  $\lambda'_{311} = 0$  and  $\lambda'_{322} \neq 0$
- case-III  $\lambda'_{311} \neq 0$  and  $\lambda'_{322} \neq 0$ .

We clarify the dependence of the couplings on various processes, and discuss the discrimination between these cases.

### III. EXOTIC PROCESSES IN THE BENCHMARK RPV SCENARIO

In the RPV scenario, we have five types of exotic processes:  $\mu - e$  conversion in a nucleus,  $pp \rightarrow \mu^- e^+$ ,  $pp \rightarrow jj$ , nonstandard interaction (NSI) of neutrinos, and muonium conversion  $\mu^+ e^- \leftrightarrow \mu^- e^+$ . We formulate each reaction rate in our benchmark scenario.

#### A. $\mu - e$ conversion

We briefly review the formulation of the branching ratio of the  $\mu - e$  conversion process based on Refs. [32,33]. The  $\mu - e$  conversion process via tau sneutrino exchange is described by the effective interaction Lagrangian

$$\mathcal{L}_{\text{int}} = -\frac{G_F}{\sqrt{2}} \sum_{q=d,s} \{ (g_{LS(q)} \bar{e} P_R \mu + g_{RS(q)} \bar{e} P_L \mu) \bar{q} q \} + \text{H.c.}, \quad (5)$$

where  $G_F$  is the Fermi coupling constant. The coefficients  $g_{LS(q)}$  and  $g_{RS(q)}$  are derived from the RPV interaction Lagrangian [Eq. (4)],

$$g_{LS(d)} = \frac{\sqrt{2}}{G_F} \frac{2}{m_{\tilde{\nu}_\tau}^2} \lambda'_{311} \lambda_{312}^*, \quad (6)$$

$$g_{RS(d)} = \frac{\sqrt{2}}{G_F} \frac{2}{m_{\tilde{\nu}_\tau}^2} \lambda_{311}'^* \lambda_{321}, \quad (7)$$

$$g_{LS(s)} = \frac{\sqrt{2}}{G_F} \frac{2}{m_{\tilde{\nu}_\tau}^2} \lambda'_{322} \lambda_{312}^*, \quad (8)$$

$$g_{RS(s)} = \frac{\sqrt{2}}{G_F} \frac{2}{m_{\tilde{\nu}_\tau}^2} \lambda_{322}'^* \lambda_{321}. \quad (9)$$

The amplitude for the  $\mu - e$  conversion process is calculated by the overlap of wave functions of the initial state muon  $\psi_{1S}^{(\mu)}$ , the final state electron  $\psi_{\kappa,W}^{\mu(e)}$  with the eigenvalues of the orbital angular momentum  $-\kappa$  and of the  $z$ -component angular momentum  $\mu$ , and the initial and final state nucleus as follows:

$$\begin{aligned} \mathcal{M} = & \frac{G_F}{\sqrt{2}} \sum_{q=d,s} \int d^3\mathbf{x} (g_{LS(q)} \bar{\psi}_{\kappa,W}^{\mu(e)} P_R \psi_{1S}^{(\mu)} \\ & + g_{RS(q)} \bar{\psi}_{\kappa,W}^{\mu(e)} P_L \psi_{1S}^{(\mu)}) \langle N | \bar{q} q | N \rangle. \end{aligned} \quad (10)$$

Here we omitted the incoherent conversion process because its fraction is much smaller than the coherent one. The matrix element  $\langle N | \bar{q} q | N \rangle$  is given by the atomic number  $Z$ , the mass number  $A$ , and the proton (neutron) density in nucleus  $\rho^{(p)}$  ( $\rho^{(n)}$ ),

$$\langle N | \bar{q} q | N \rangle = Z G_S^{(q,p)} \rho^{(p)} + (A - Z) G_S^{(q,n)} \rho^{(n)}. \quad (11)$$

The coefficients for scalar operators are evaluated in Ref. [34]:  $G_S^{(d,n)} = 5.1$ ,  $G_S^{(d,p)} = 4.3$ , and  $G_S^{(s,p)} = G_S^{(s,n)} = 2.5$ . This calculation assumes that the proton and the neutron densities are in spherical distribution and normalized as  $\int dr 4\pi r^2 \rho^{(p,n)} = 1$ .

The reaction rate of the  $\mu - e$  conversion is

$$\begin{aligned} \omega_{\text{conv}} = & 2G_F^2 |\tilde{g}_{LS}^{(p)} S^{(p)} + \tilde{g}_{LS}^{(n)} S^{(n)}|^2 \\ & + 2G_F^2 |\tilde{g}_{RS}^{(p)} S^{(p)} + \tilde{g}_{RS}^{(n)} S^{(n)}|^2. \end{aligned} \quad (12)$$

$$\begin{aligned} \omega_{\text{conv}} = & \frac{16}{m_{\tilde{\nu}_\tau}^4} |(4.3S^{(p)} + 5.1S^{(n)}) \lambda'_{311} \lambda_{312}^* + 2.5(S^{(p)} + S^{(n)}) \lambda'_{322} \lambda_{312}^*|^2 \\ & + \frac{16}{m_{\tilde{\nu}_\tau}^4} |(4.3S^{(p)} + 5.1S^{(n)}) \lambda_{311}' \lambda_{321}^* + 2.5(S^{(p)} + S^{(n)}) \lambda_{322}' \lambda_{321}^*|^2. \end{aligned} \quad (15)$$

The branching ratio of the  $\mu - e$  conversion process is defined by

$$\text{BR}(\mu^- N \rightarrow e^- N) = \omega_{\text{conv}} / \omega_{\text{capt}}, \quad (16)$$

where  $\omega_{\text{capt}}$  is the muon capture rate of the nucleus. We list the values of  $\omega_{\text{capt}}$  in Table I. Assuming  $\lambda'_{311}$  and  $\lambda'_{322}$  are real and  $\lambda_{312}^* = \lambda_{321} \equiv \lambda$ , the branching ratio for  $N = \text{C}$  is given by

$$\begin{aligned} \text{BR}(\mu^- \text{C} \rightarrow e^- \text{C}) = & 1.383 \times 10^{-15} \left( \frac{1 \text{ TeV}}{m_{\tilde{\nu}_\tau}} \right)^4 \left( \frac{\lambda'_{311} \lambda}{10^{-8}} \right)^2 \left| 1 + 0.532 \left( \frac{\lambda'_{322}}{\lambda'_{311}} \right) \right|^2 \\ = & 3.913 \times 10^{-16} \left( \frac{1 \text{ TeV}}{m_{\tilde{\nu}_\tau}} \right)^4 \left( \frac{\lambda'_{322} \lambda}{10^{-8}} \right)^2 \left| 1 + 1.880 \left( \frac{\lambda'_{311}}{\lambda'_{322}} \right) \right|^2, \end{aligned} \quad (17)$$

for  $N = \text{Al}$ ,

TABLE I. The overlap factor of wave functions (explicit formulas and details of the calculation are explained in Ref. [33]) and the muon capture rate  $\omega_{\text{capt}}$  for each nucleus. Here  $m_\mu$  is muon mass.

Nucleus	$S^{(p)}$	$S^{(n)}$	$\omega_{\text{capt}} (s^{-1})$
C	$0.00308 m_\mu^{5/2}$	$0.00308 m_\mu^{5/2}$	$0.388 \times 10^5$
Si	$0.0179 m_\mu^{5/2}$	$0.0179 m_\mu^{5/2}$	$8.712 \times 10^5$
Al	$0.0155 m_\mu^{5/2}$	$0.0167 m_\mu^{5/2}$	$7.054 \times 10^5$
Ti	$0.0368 m_\mu^{5/2}$	$0.0435 m_\mu^{5/2}$	$2.590 \times 10^6$
Au	$0.0614 m_\mu^{5/2}$	$0.0918 m_\mu^{5/2}$	$1.307 \times 10^7$

The overlap integral of the wave functions of the muon, electron, and protons (neutrons) gives  $S^{(p)}$  ( $S^{(n)}$ ) (explicit formulas and details of the calculation are explained in Ref. [33]). We list  $S^{(p)}$  and  $S^{(n)}$  for relevant nuclei of SINDRUM-II (Au), DeeMe (C and Si), COMET (Al and Ti), Mu2e (Al and Ti), and PRISM (Al and Ti) in Table I. The coefficients  $\tilde{g}_{LS,RS}^{(p)}$  and  $\tilde{g}_{LS,RS}^{(n)}$  are

$$\tilde{g}_{LS,RS}^{(p)} = \sum_q G_S^{q,p} g_{LS,RS(q)} = G_S^{d,p} g_{LS,RS(d)} + G_S^{s,p} g_{LS,RS(s)}, \quad (13)$$

$$\tilde{g}_{LS,RS}^{(n)} = \sum_q G_S^{q,n} g_{LS,RS(q)} = G_S^{d,n} g_{LS,RS(d)} + G_S^{s,n} g_{LS,RS(s)}. \quad (14)$$

Thus, the reaction rate of  $\mu - e$  conversion via the  $\tilde{\nu}_\tau$  exchange is obtained as follows:

$$\begin{aligned} \text{BR}(\mu^- \text{Al} \rightarrow e^- \text{Al}) &= 2.092 \times 10^{-15} \left( \frac{1 \text{ TeV}}{m_{\tilde{\nu}_\tau}} \right)^4 \left( \frac{\lambda'_{311} \lambda}{10^{-8}} \right)^2 \left| 1 + 0.530 \left( \frac{\lambda'_{322}}{\lambda'_{311}} \right) \right|^2 \\ &= 5.881 \times 10^{-16} \left( \frac{1 \text{ TeV}}{m_{\tilde{\nu}_\tau}} \right)^4 \left( \frac{\lambda'_{322} \lambda}{10^{-8}} \right)^2 \left| 1 + 1.886 \left( \frac{\lambda'_{311}}{\lambda'_{322}} \right) \right|^2, \end{aligned} \quad (18)$$

for  $N = \text{Si}$ ,

$$\begin{aligned} \text{BR}(\mu^- \text{Si} \rightarrow e^- \text{Si}) &= 2.080 \times 10^{-15} \left( \frac{1 \text{ TeV}}{m_{\tilde{\nu}_\tau}} \right)^4 \left( \frac{\lambda'_{311} \lambda}{10^{-8}} \right)^2 \left| 1 + 0.532 \left( \frac{\lambda'_{322}}{\lambda'_{311}} \right) \right|^2 \\ &= 5.886 \times 10^{-16} \left( \frac{1 \text{ TeV}}{m_{\tilde{\nu}_\tau}} \right)^4 \left( \frac{\lambda'_{322} \lambda}{10^{-8}} \right)^2 \left| 1 + 1.880 \left( \frac{\lambda'_{311}}{\lambda'_{322}} \right) \right|^2, \end{aligned} \quad (19)$$

and for  $N = \text{Ti}$ ,

$$\begin{aligned} \text{BR}(\mu^- \text{Ti} \rightarrow e^- \text{Ti}) &= 3.571 \times 10^{-15} \left( \frac{1 \text{ TeV}}{m_{\tilde{\nu}_\tau}} \right)^4 \left( \frac{\lambda'_{311} \lambda}{10^{-8}} \right)^2 \left| 1 + 0.528 \left( \frac{\lambda'_{322}}{\lambda'_{311}} \right) \right|^2 \\ &= 9.962 \times 10^{-16} \left( \frac{1 \text{ TeV}}{m_{\tilde{\nu}_\tau}} \right)^4 \left( \frac{\lambda'_{322} \lambda}{10^{-8}} \right)^2 \left| 1 + 1.893 \left( \frac{\lambda'_{311}}{\lambda'_{322}} \right) \right|^2. \end{aligned} \quad (20)$$

### B. $pp \rightarrow \mu^- e^+$ and $pp \rightarrow jj$

We formulate the cross sections of  $pp \rightarrow \mu^- e^+$  and  $pp \rightarrow jj$  in the RPV scenario. In the scenario, these processes are dominated by the  $s$ -channel exchange resonance, and hence the cross sections are well approximated by the Breit-Wigner formula. The cross section for a final state  $f_1 f_2$  is decomposed with  $\gamma_{\tilde{\nu}_\tau} = \Gamma_{\tilde{\nu}_\tau} / m_{\tilde{\nu}_\tau}$  as follows:

$$\begin{aligned} \sigma(pp \rightarrow f_1 f_2) &= F(\sqrt{s}, m_{\tilde{\nu}_\tau}, q_1, q_2) \times \Gamma_{\tilde{\nu}_\tau} \text{BR}(\tilde{\nu}_\tau \rightarrow q_1 q_2) \text{BR}(\tilde{\nu}_\tau \rightarrow f_1 f_2) \\ &= F(\sqrt{s}, m_{\tilde{\nu}_\tau}, q_1, q_2) m_{\tilde{\nu}_\tau} \times \gamma_{\tilde{\nu}_\tau} \text{BR}(\tilde{\nu}_\tau \rightarrow q_1 q_2) \text{BR}(\tilde{\nu}_\tau \rightarrow f_1 f_2). \end{aligned} \quad (21)$$

The front part,  $F(\sqrt{s}, m_{\tilde{\nu}_\tau}, q_1, q_2) m_{\tilde{\nu}_\tau}$ , is determined by the kinematics of each process and is a function of collision energy  $\sqrt{s}$ , mediator mass  $m_{\tilde{\nu}_\tau}$ , and the flavors of initial quarks ( $q_1$  and  $q_2$ ). The decay width  $\Gamma_{\tilde{\nu}_{tL}}$  is calculated by the Lagrangian [Eq. (4)],

$$\Gamma_{\tilde{\nu}_{tL}} = \frac{m_{\tilde{\nu}_{tL}}}{16\pi} (3\lambda_{311}^{\prime 2} + 3\lambda_{322}^{\prime 2} + 4\lambda_{312}^{\prime 2} + 4\lambda_{321}^{\prime 2}). \quad (22)$$

The remaining part,  $\gamma_{\tilde{\nu}_\tau} \text{BR}(\tilde{\nu}_\tau \rightarrow q_1 q_2) \text{BR}(\tilde{\nu}_\tau \rightarrow f_1 f_2)$ , depends only on the coupling constants of the RPV interactions.

First we formulate  $F(\sqrt{s}, m_{\tilde{\nu}_\tau}, q_1, q_2)$ . Regardless of the final state, once  $\sqrt{s}$ ,  $m_{\tilde{\nu}_\tau}$ , and an initial state are fixed,  $F(\sqrt{s}, m_{\tilde{\nu}_\tau}, q_1, q_2)$  is uniquely determined. It is really important and useful for analyzing the RPV coupling dependence on the cross sections to derive the explicit formula of  $F(\sqrt{s}, m_{\tilde{\nu}_\tau}, q_1, q_2)$ . The expression of  $F(\sqrt{s}, m_{\tilde{\nu}_\tau}, q_1, q_2)$  is given from Eq. (21),

$$F(\sqrt{s}, m_{\tilde{\nu}_\tau}, q_1, q_2) = \frac{\sigma(pp \rightarrow f_1 f_2)}{m_{\tilde{\nu}_\tau} \gamma_{\tilde{\nu}_\tau} \text{BR}(\tilde{\nu}_\tau \rightarrow q_1 q_2) \text{BR}(\tilde{\nu}_\tau \rightarrow f_1 f_2)}. \quad (23)$$

Numerical results from Eq. (23) are shown by rotated squares in Fig. 3. In Fig. 3, we use the abbreviation  $F_{q_1 q_2}$  as  $F(\sqrt{s}, m_{\tilde{\nu}_\tau}, q_1, q_2)$ . For each set of  $\sqrt{s}$  and initial state quarks, we can parametrize  $F(\sqrt{s}, m_{\tilde{\nu}_\tau}, q_1, q_2)$  as a function of  $m_{\tilde{\nu}_\tau}$  as follows,

$$F(\sqrt{s}, m_{\tilde{\nu}_\tau}, q_1, q_2) = \alpha \times 10^{-\beta m_{\tilde{\nu}_\tau}} m_{\tilde{\nu}_\tau}^{-\gamma} [\text{pb} \cdot \text{GeV}^{-1}], \quad (24)$$

where coefficients  $\alpha$ ,  $\beta$ , and  $\gamma$  are calculated from numerical calculations of  $F(\sqrt{s}, m_{\tilde{\nu}_\tau}, q_1, q_2)$ , and we list the coefficients in Table II. The fitted function of  $F(\sqrt{s}, m_{\tilde{\nu}_\tau}, q_1, q_2)$  for collision energy  $\sqrt{s} = 14$  and  $\sqrt{s} = 100$  TeV are shown by lines in Fig. 3.

From Eq. (21), the cross section of  $pp \rightarrow \mu^- e^+$  is analytically calculated with the decay rate [Eq. (22)] and the fit function of  $F(\sqrt{s}, m_{\tilde{\nu}_\tau}, q_1, q_2)$  [Eq. (24)] as follows:

$$\sigma(pp \rightarrow \mu^- e^+) = \sum_{i=1,2} \left\{ F(\sqrt{s}, m_{\tilde{\nu}_\tau}, d_i, \bar{d}_i) m_{\tilde{\nu}_\tau} \times \frac{1}{16\pi} (3\lambda_{311}^2 + 3\lambda_{322}^2 + 4\lambda_{312}^2 + 4\lambda_{321}^2) \right. \\ \left. \times \frac{3\lambda_{3ii}^2}{3\lambda_{311}^2 + 3\lambda_{322}^2 + 4\lambda_{312}^2 + 4\lambda_{321}^2} \cdot \frac{4\lambda_{312}^2}{3\lambda_{311}^2 + 3\lambda_{322}^2 + 4\lambda_{312}^2 + 4\lambda_{321}^2} \right\}. \quad (25)$$

Here  $d_1 = d$  and  $d_2 = s$ . The cross section of dijet production,  $\sigma(pp \rightarrow jj)$ , is similarly calculated as follows:<sup>2</sup>

$$\sigma(pp \rightarrow jj) = \frac{9}{16\pi} \left\{ F_{d\bar{d}} + F_{u\bar{d}} + F_{\bar{u}d} \right\} m_{\tilde{\nu}_\tau} \times \frac{\lambda_{311}^4}{3\lambda_{311}^2 + 3\lambda_{322}^2 + 4\lambda_{312}^2 + 4\lambda_{321}^2} + \frac{9}{16\pi} \left\{ F_{d\bar{d}} + F_{u\bar{d}} + F_{\bar{u}d} + F_{s\bar{s}} \right\} m_{\tilde{\nu}_\tau} \\ \times \frac{\lambda_{311}^2 \lambda_{322}^2}{3\lambda_{311}^2 + 3\lambda_{322}^2 + 4\lambda_{312}^2 + 4\lambda_{321}^2} + \frac{9}{16\pi} \left\{ F_{s\bar{s}} \right\} m_{\tilde{\nu}_\tau} \times \frac{\lambda_{322}^4}{3\lambda_{311}^2 + 3\lambda_{322}^2 + 4\lambda_{312}^2 + 4\lambda_{321}^2}. \quad (26)$$

The terms of  $F_{u\bar{d}}$  and  $F_{\bar{u}d}$  are the left-handed stau exchange contributions. Since the tau sneutrino and the stau are components of the  $SU(2)_L$  doublet, we assumed their degeneracy in mass. In case I (case II), only the first line (third line) contributes to the dijet production.

### C. NSI

With the interaction Eq. (4), there is modification of the neutrino oscillation physics. It is called nonstandard interaction (NSI). In particular, there is a strong enhancement, called a chiral enhancement.

Conventional beam experiments use neutrinos emitted by  $\pi$  decay. In the presence of the interaction Eq. (4), we have an effective operator which causes a  $\pi$  decay with LFV in the following way:

The effective Lagrangian is

$$\mathcal{L} = \frac{2\lambda_{312}^* \lambda'_{311}}{m_{\tilde{\tau}}^2} \bar{\nu}_e \mu_R \bar{d}_R u_L + \frac{2\lambda_{321}^* \lambda'_{311}}{m_{\tilde{\tau}}^2} \bar{\nu}_\mu e_R \bar{d}_R u_L + \text{H.c.} \quad (27)$$

The amplitude for  $\pi^+ \rightarrow \mu^+ \nu_e$  is proportional to

$$\mathcal{M} \propto \langle \nu_e \mu^+ | \bar{\nu}_e \mu_R | 0 \rangle \langle 0 | \bar{d}_R u_L | \pi^+ \rangle. \quad (28)$$

Since [36]

$$\bar{d}_R u_L = \frac{i}{m} \partial_\mu (\bar{u} \gamma^\mu \gamma_5 d) \quad (29)$$

using the equation of motion, and  $m = m_u + m_d$ , a sum of  $u$ - and  $d$ -quark masses. Therefore, the magnitude of the amplitude is enhanced by [37]

<sup>2</sup>Both the  $s$ -channel and  $t$ -channel  $\tilde{\nu}_{\tau_L}$  ( $\tilde{\tau}_L$ ) exchange processes contribute the dijet production in our scenario. Since the  $s$ -channel processes are highly dominant, we can formulate  $\sigma(pp \rightarrow jj)$  with the Breit-Wigner formula.

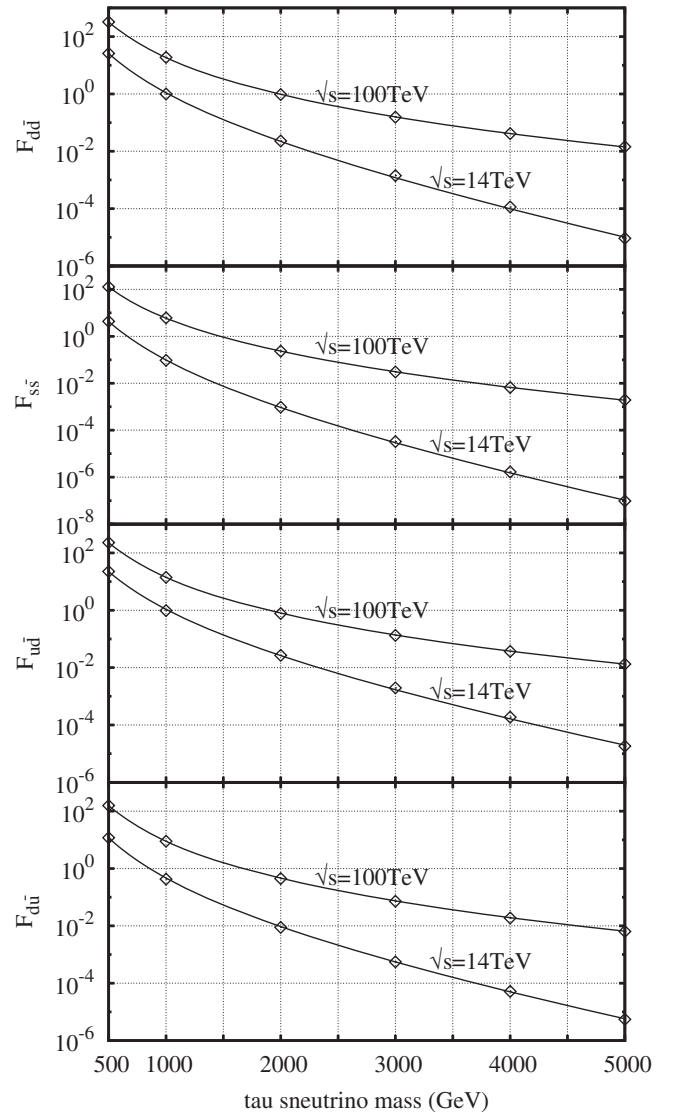


FIG. 3. Fit functions and numerical results of  $F(\sqrt{s}, m_{\tilde{\nu}_\tau}, q_1, q_2)$  for collision energy  $\sqrt{s} = 14$  and  $\sqrt{s} = 100$  TeV. Rotated squares are numerical results calculated from Eq. (23), and lines are fit functions.

TABLE II. The coefficients for fit function of  $F(\sqrt{s}, m_{\bar{\nu}_\tau}, q_1, q_2)$  [see Eq. (23)] for each set of the collision energy  $\sqrt{s}$  and initial state quarks. We use the CTEQ6L parton distribution function [35] for the evaluation.

$(\sqrt{s}(\text{TeV}), q_1, q_2)$	$\alpha$ [pb · GeV $^{\gamma-1}$ ]	$\beta$ [GeV $^{-1}$ ]	$\gamma$
(14, $d, \bar{d}$ )	$1.352 \times 10^{11}$	$6.500 \times 10^{-4}$	3.480
(14, $u, \bar{d}$ )	$6.652 \times 10^{10}$	$5.900 \times 10^{-4}$	3.400
(14, $d, \bar{u}$ )	$2.233 \times 10^{11}$	$5.800 \times 10^{-4}$	3.700
(14, $s, \bar{s}$ )	$2.248 \times 10^{12}$	$7.600 \times 10^{-4}$	4.200
(100, $d, \bar{d}$ )	$2.220 \times 10^{13}$	$8.000 \times 10^{-5}$	4.000
(100, $u, \bar{d}$ )	$8.385 \times 10^{12}$	$7.500 \times 10^{-5}$	3.900
(100, $d, \bar{u}$ )	$1.084 \times 10^{13}$	$8.500 \times 10^{-5}$	4.000
(100, $s, \bar{s}$ )	$3.265 \times 10^{13}$	$1.400 \times 10^{-4}$	4.200

$$\frac{m_\pi^2}{m_\mu m}, \quad (30)$$

compared with the usual current-current interaction. Here,  $m_\pi$  is the  $\pi$  mass. This is the chiral enhancement. We can expect 30 times the enhancement. It interferes with the usual  $\pi$  decay, though it depends on the phase of  $\lambda_{312}^* \lambda'_{311}$  and can affect the neutrino oscillation experiment with conventional beam.

The strength of the NSIs is parametrized by the relative strength with the weak interaction. For the conventional beam experiment, the effect of  $\pi^+ \rightarrow \mu^+ \nu_e$  is denoted by  $\epsilon_{\mu e}^S$  and

$$\epsilon_{\mu e}^S = \sqrt{2} \frac{m_\pi^2}{m_\mu m} \frac{2\lambda_{312}^* \lambda'_{311}}{G_F m_\tau^2}. \quad (31)$$

With this interaction, the  $\mu$  flavor eigenstate in the  $\pi$  decay, which is denoted by (0,1,0) in the lepton flavor eigenstates, is deformed to be  $(\epsilon_{\mu e}^S, 1, 0)$ .

Note that the operator  $\bar{e}_R \nu_\mu \bar{u}_L d_R$  causes  $\pi^- \rightarrow e^- \bar{\nu}_\mu$ . It has an electron final state. Since there is  $\mu$  in the  $\pi$  decay in more than 99% of the cases, it cannot interfere with a usual  $\pi$  decay and, hence, it has no effect on neutrino oscillation experiments. Furthermore, the  $\pi$  decay cannot be caused by operators with  $\lambda'_{322}$ . It means, in principle, the operator with  $\lambda_{312} \lambda'_{311}$  can be distinguished from others in neutrino oscillation experiments.

In principle, there are other NSI processes in the matter effect and detection process. They are, however, absent or tiny. Indeed, there is no matter effect as  $\lambda'_{311}$  is absent. The NSI effect detection process is suppressed by chirality since the interaction is not the (V-A)(V-A) type [38].

### D. Muonium conversion

In the scenario, muonium ( $M = \mu^+ e^-$ ) converts to antimuonium ( $\bar{M} = \mu^- e^+$ ) via the tau sneutrino exchange. The  $M-\bar{M}$  conversion is described by the  $(V \pm A) \times (V \pm A)$  form interaction [39]

$$\mathcal{L}(M \rightarrow \bar{M}) = \frac{G_{M\bar{M}}}{\sqrt{2}} (\bar{\mu} \gamma_\mu P_L e) (\bar{\mu} \gamma^\mu P_R e) + \text{H.c.} \quad (32)$$

Here,  $G_{M\bar{M}}$  is an effective coupling analogous to the Fermi coupling constant  $G_F$ . The latest experimental limit of the  $M-\bar{M}$  conversion is set on the  $G_{M\bar{M}}$ ,  $G_{M\bar{M}} \leq 3.0 \times 10^{-3} G_F$  [40]. We derive the interaction Lagrangian describing the  $M-\bar{M}$  conversion by the Fierz transformation from the fundamental Lagrangian (4) as follows:

$$\mathcal{L}(M \rightarrow \bar{M}) = \frac{\lambda_{321} \lambda_{312}^*}{2m_{\bar{\nu}_\tau}^2} (\bar{\mu} \gamma_\mu P_L e) (\bar{\mu} \gamma^\mu P_R e) + \text{H.c.} \quad (33)$$

Thus, the upper bound from the  $M-\bar{M}$  conversion search experiment is

$$|\lambda_{321} \lambda_{312}^*| \left( \frac{1 \text{ TeV}}{m_{\bar{\nu}_\tau}} \right)^2 \leq 4.948 \times 10^{-2}. \quad (34)$$

## IV. NUMERICAL RESULT

We are now in a position to show numerical results. Table III shows the current experimental limit and the future single event sensitivity for the  $\mu-e$  conversion process. It also shows the upper limits on the combination of the RPV couplings,  $\lambda' \lambda$ , corresponding to the limit and the sensitivities. In the calculation of the upper limits, we take Au, Si, and Al for the target nucleus of SINDRUM-II, DeeMe, and other experiments, respectively.

The  $\mu-e$  conversion search is a reliable probe for both the RPV couplings and tau sneutrino mass. The current experimental limit puts strict limits on the RPV couplings,  $\lambda' \lambda \lesssim 10^{-7}$  for  $m_{\bar{\nu}_\tau} = 1 \text{ TeV}$  and  $\lambda' \lambda \lesssim 10^{-5}$  for  $m_{\bar{\nu}_\tau} = 3 \text{ TeV}$ , respectively. In the near future, the accessible RPV couplings will be extended by more than 3 orders of current limits,  $\lambda' \lambda \approx 10^{-10}$  for  $m_{\bar{\nu}_\tau} = 1 \text{ TeV}$  and  $\lambda' \lambda \approx 10^{-8}$  for  $m_{\bar{\nu}_\tau} = 3 \text{ TeV}$ , respectively.

The  $\mu-e$  conversion process is one of the clear signatures for the RPV scenario, but it is not sufficient evidence for the scenario. We must check the correlations among the reaction rates of the  $\mu-e$  conversion process, the cross sections of  $pp \rightarrow \mu^- e^+$  and  $pp \rightarrow jj$ , and so on in order to discriminate case I, II, and III from each other and confirm the RPV scenario. In the following subsections, in each case, we show the correlations and discuss the parameter determination.

### A. Case I ( $\lambda'_{311} \neq 0, \lambda'_{322} = 0$ )

The parameter dependence of  $\sigma(pp \rightarrow \mu^- e^+)$ ,  $\sigma(pp \rightarrow jj)$ , and  $\text{BR}(\mu^- N \rightarrow e^- N)$  are depicted in Fig. 4. Dashed and dot-dashed lines are contours of  $\sigma(pp \rightarrow \mu^- e^+)$  and  $\sigma(pp \rightarrow jj)$  at  $\sqrt{s} = 14 \text{ TeV}$  (left panels) and  $\sqrt{s} = 100 \text{ TeV}$  (right panels), respectively. Solid lines are contours of  $\text{BR}(\mu^- \text{Al} \rightarrow e^- \text{Al})$ , which are

TABLE III. Current and future experimental limits on the  $\mu$ - $e$  conversion branching ratio and the upper limits on  $\lambda'\lambda$  corresponding to each experimental limit.

Experiment	BR limit	Limit on $\lambda'_{311}\lambda$ (case I)	Limit on $\lambda'_{322}\lambda$ (case II)	Limit on $\lambda'\lambda$ (case III)
SINDRUM	$7 \times 10^{-13}$ [4]	$1.633 \times 10^{-7} \left(\frac{m_{\tilde{\nu}_\tau}}{1 \text{ TeV}}\right)^2$	$3.170 \times 10^{-7} \left(\frac{m_{\tilde{\nu}_\tau}}{1 \text{ TeV}}\right)^2$	$1.072 \times 10^{-7} \left(\frac{m_{\tilde{\nu}_\tau}}{1 \text{ TeV}}\right)^2$
DeeMe	$5 \times 10^{-15}$ [15]	$1.550 \times 10^{-8} \left(\frac{m_{\tilde{\nu}_\tau}}{1 \text{ TeV}}\right)^2$	$2.915 \times 10^{-8} \left(\frac{m_{\tilde{\nu}_\tau}}{1 \text{ TeV}}\right)^2$	$1.012 \times 10^{-8} \left(\frac{m_{\tilde{\nu}_\tau}}{1 \text{ TeV}}\right)^2$
COMET-I	$7 \times 10^{-15}$ [14]	$1.830 \times 10^{-8} \left(\frac{m_{\tilde{\nu}_\tau}}{1 \text{ TeV}}\right)^2$	$3.504 \times 10^{-8} \left(\frac{m_{\tilde{\nu}_\tau}}{1 \text{ TeV}}\right)^2$	$1.196 \times 10^{-8} \left(\frac{m_{\tilde{\nu}_\tau}}{1 \text{ TeV}}\right)^2$
COMET-II	$3 \times 10^{-17}$ [14]	$1.198 \times 10^{-9} \left(\frac{m_{\tilde{\nu}_\tau}}{1 \text{ TeV}}\right)^2$	$2.294 \times 10^{-9} \left(\frac{m_{\tilde{\nu}_\tau}}{1 \text{ TeV}}\right)^2$	$7.827 \times 10^{-10} \left(\frac{m_{\tilde{\nu}_\tau}}{1 \text{ TeV}}\right)^2$
PRISM	$7 \times 10^{-19}$ [14]	$1.830 \times 10^{-10} \left(\frac{m_{\tilde{\nu}_\tau}}{1 \text{ TeV}}\right)^2$	$3.504 \times 10^{-10} \left(\frac{m_{\tilde{\nu}_\tau}}{1 \text{ TeV}}\right)^2$	$1.196 \times 10^{-10} \left(\frac{m_{\tilde{\nu}_\tau}}{1 \text{ TeV}}\right)^2$

translated from the single event sensitivities of each experiment (see Table III). Light-shaded region is excluded by the  $\mu$ - $e$  conversion search at the SINDRUM-II experiment [4], and the dark-shaded band is the excluded region in the  $M$ - $\bar{M}$  conversion search experiment at the Paul Scherrer Institute (PSI) [40]. We take  $m_{\tilde{\nu}_\tau} = 1 \text{ TeV}$  for panels (a) and (b), and  $m_{\tilde{\nu}_\tau} = 3$  for panels (c) and (d). For simplicity, we take the couplings universally in the leptonic RPV sector:  $\lambda \equiv \lambda_{312} = \lambda_{321} = -\lambda_{132} = -\lambda_{231}$ .

Figure 4 displays the strong potential of the  $\mu$ - $e$  conversion search to explore the RPV scenarios. The PRISM experiment will cover almost parameter space which the LHC experiment can survey. In the parameter range between the SINDRUM-II limit and the PRISM reach, combining the measurement results of  $\sigma(pp \rightarrow \mu^- e^+)$ ,  $\sigma(pp \rightarrow jj)$ , and  $\text{BR}(\mu^- \text{Al} \rightarrow e^- \text{Al})$ , the RPV couplings and the tau sneutrino mass will be precisely determined.

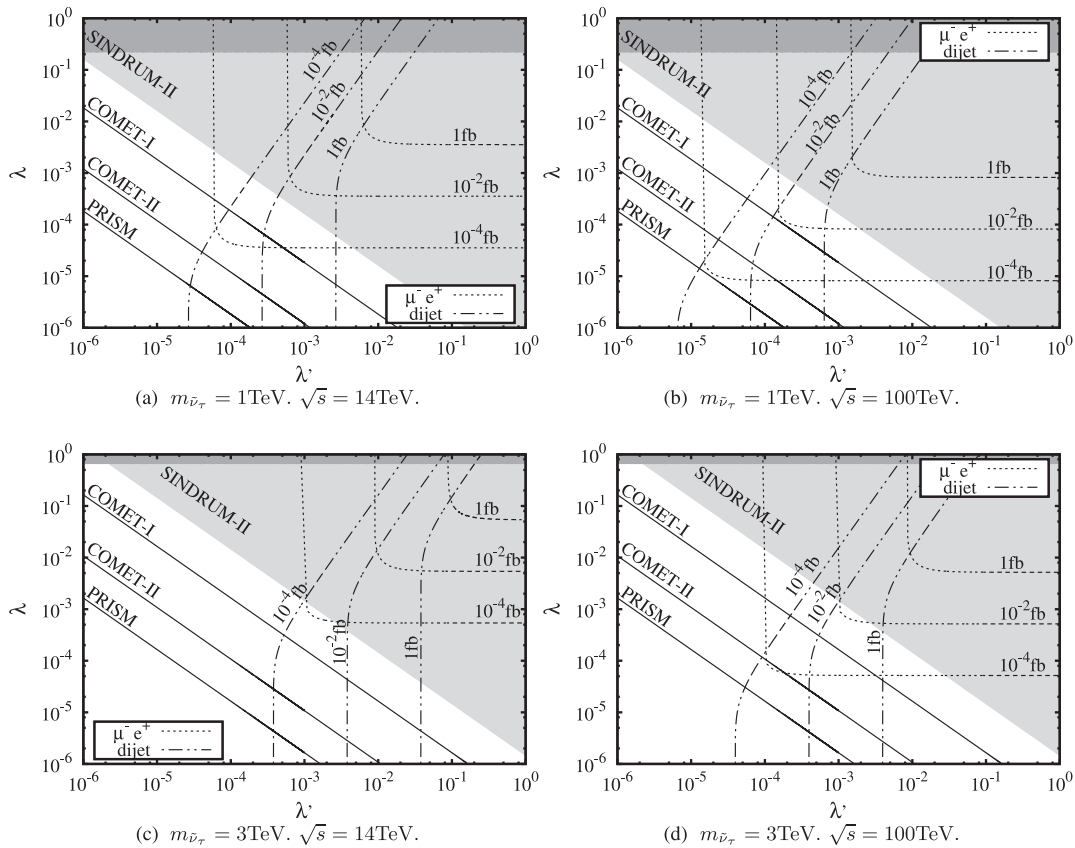


FIG. 4. Contour plot of  $\sigma(pp \rightarrow \mu^- e^+)$ ,  $\sigma(pp \rightarrow \text{dijet})$ , and  $\text{BR}(\mu^- N \rightarrow e^- N)$  in case I for (a)  $m_{\tilde{\nu}_\tau} = 1 \text{ TeV}$  and  $\sqrt{s} = 14 \text{ TeV}$ , (b)  $m_{\tilde{\nu}_\tau} = 1 \text{ TeV}$  and  $\sqrt{s} = 100 \text{ TeV}$ , (c)  $m_{\tilde{\nu}_\tau} = 3 \text{ TeV}$  and  $\sqrt{s} = 14 \text{ TeV}$ , (d)  $m_{\tilde{\nu}_\tau} = 3 \text{ TeV}$  and  $\sqrt{s} = 100 \text{ TeV}$ . For simplicity, we take the universal RPV coupling,  $\lambda \equiv \lambda_{312} = \lambda_{321} = -\lambda_{132} = -\lambda_{231}$ . The light-shaded region is excluded by the  $\mu$ - $e$  conversion search [4], and the dark-shaded band is the excluded region by the  $M$ - $\bar{M}$  conversion search [40].

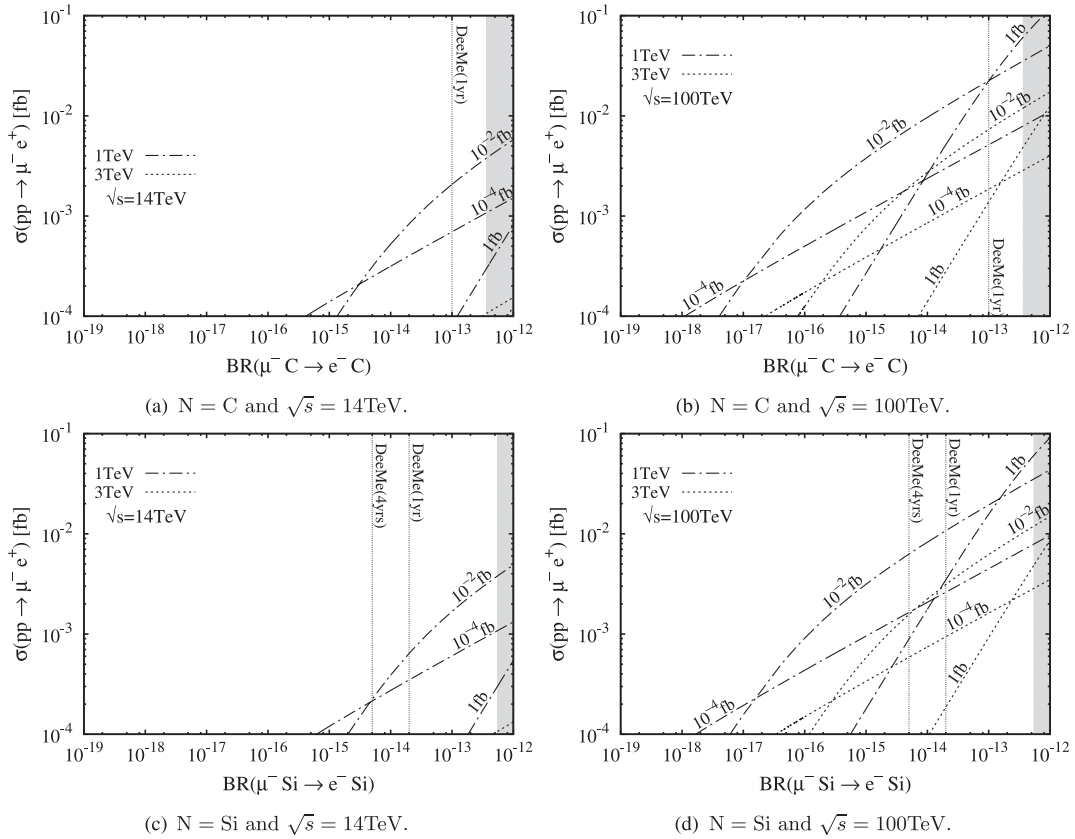


FIG. 5.  $\sigma(pp \rightarrow \mu^- e^+)$  as a function of  $\text{BR}(\mu^- N \rightarrow e^- N)$  for each  $\sigma(pp \rightarrow jj)$  in case I.  $\sigma(pp \rightarrow jj)$  are attached on each line. Results for  $m_{\tilde{\nu}_\tau} = 1$  TeV ( $m_{\tilde{\nu}_\tau} = 3$  TeV) are given by the dot-dashed line (dotted line). Shaded region in each panel is the excluded region by the SINDRUM-II experiment. Left panels show the results for the collision energy  $\sqrt{s} = 14$  TeV, and right panels show the results for  $\sqrt{s} = 100$  TeV. We take C [(a) and (b)], and Si [(c) and (d)] for the target nucleus of the  $\mu$ - $e$  conversion process.

Figures 5 and 6 show  $\sigma(pp \rightarrow \mu\bar{e})$  as a function of  $\text{BR}(\mu + N \rightarrow e + N)$  in case I. Candidate materials for the target of the  $\mu$ - $e$  conversion search are carbon (C) and silicon (Si) at the DeeMe experiment, and are aluminum (Al) or titanium (Ti) at the COMET, Mu2e, and PRISM experiment. Vertical dotted lines show the experimental reach of DeeMe 1-year running [DeeMe(1 yr)], DeeMe 4-years running [DeeMe(4 yrs)], COMET phase I (COMET-I), COMET phase II (COMET-II), and PRISM (PRISM). Shaded regions are the excluded region by the SINDRUM-II experiment [4], which are translated into the limit for each nucleus from that for Au. The experimental reach of the Mu2e experiment is planned to be close to that of COMET phase II [41]. Left and right panels show the results of  $\sqrt{s} = 14$  and  $\sqrt{s} = 100$  TeV, respectively. Results for  $m_{\tilde{\nu}_\tau} = 1$  and  $m_{\tilde{\nu}_\tau} = 3$  TeV are given by the dot-dashed line and dotted line, respectively. Each line corresponds to the dijet production cross section at the LHC,  $\sigma(pp \rightarrow jj)$ , at  $\sqrt{s} = 14$  TeV (left panels) and at  $\sqrt{s} = 100$  TeV (right panels), respectively. For simplicity, we take the universal RPV coupling,  $\lambda \equiv \lambda_{312} = \lambda_{321} = -\lambda_{132} = -\lambda_{231}$ .

Figures 5 and 6 show the clear correlations among  $\sigma(pp \rightarrow \mu^- e^+)$ ,  $\sigma(pp \rightarrow jj)$ , and  $\text{BR}(\mu^- N \rightarrow e^- N)$ . Checking the correlations makes it possible to distinguish the RPV scenario and other new physics scenarios.

In Figs. 5 and 6, behavior of the correlations is not so intuitive. We quantitatively analyze the behavior. We infer the  $\sigma(pp \rightarrow \mu^- e^+)$  from the  $\sigma(pp \rightarrow jj)$  and  $\text{BR}(\mu^- N \rightarrow e^- N)$ .

As we formulated in Secs. III A and III B,  $\text{BR} \equiv \text{BR}(\mu^- N \rightarrow e^- N)$  and  $\sigma_{\text{jet}} \equiv \sigma(pp \rightarrow jj)$  are divided into the kinematics part and the RPV coupling-dependent part as follows:

$$\text{BR} = k_N (\lambda'_{311} \lambda)^2, \quad (35)$$

$$\sigma_{\text{jet}} \equiv \sigma(pp \rightarrow jj) = F_{\text{jet}} \frac{\lambda_{311}^4}{3\lambda_{311}^2 + 8\lambda^2}. \quad (36)$$

Here  $k_N$  is a coefficient depending on a target nucleus  $N$  and the sneutrino mass, the values of which are calculated by Eqs. (17)–(20) and are listed in Table IV.  $F_{\text{jet}}$  includes the numerical factor and kinematical factor in

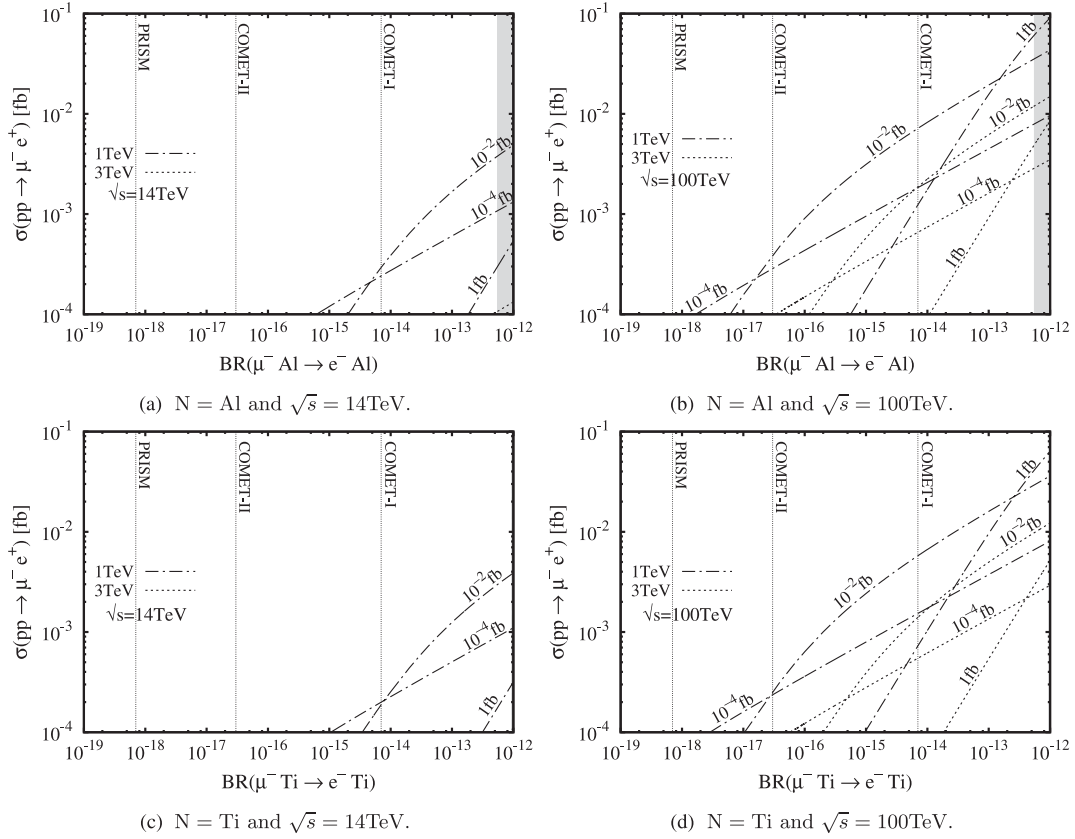


FIG. 6. Same as Fig. 5 except for target nucleus. We take Al [(a) and (b)] and Ti [(c) and (d)] for the target nucleus of the  $\mu$ - $e$  conversion process.

$\sigma_{\text{jet}}$  and is calculated from Eq. (26),  $F_{\text{jet}} = \frac{9}{16\pi} \{F_{d\bar{d}} + F_{u\bar{d}} + F_{\bar{u}d}\} m_{\bar{\nu}_\tau}$ . We have a cubic equation of  $\lambda_{311}'^2$  from Eqs. (35) and (36),

$$k_N F_{\text{jet}} (\lambda_{311}'^2)^3 - 3k_N (\lambda_{311}'^2)^2 - 8\sigma_{\text{jet}} \text{BR} = 0. \quad (37)$$

By solving the cubic equation, we obtain an analytic expression of  $\lambda_{311}'^2$  as a function of BR,

$$\begin{aligned} \lambda_{311}'^2 = & \left\{ \left( \frac{2\sigma_{\text{jet}} \text{BR}}{k_N F_{\text{jet}}} \right) + \left( \frac{\sigma_{\text{jet}}}{F_{\text{jet}}} \right)^3 + \sqrt{\left( \frac{2\sigma_{\text{jet}} \text{BR}}{k_N F_{\text{jet}}} + \left( \frac{\sigma_{\text{jet}}}{F_{\text{jet}}} \right)^3 \right)^2 - \left( \frac{\sigma_{\text{jet}}}{F_{\text{jet}}} \right)^6} \right\}^{1/3} \\ & + \left\{ \left( \frac{2\sigma_{\text{jet}} \text{BR}}{k_N F_{\text{jet}}} \right) + \left( \frac{\sigma_{\text{jet}}}{F_{\text{jet}}} \right)^3 - \sqrt{\left( \frac{2\sigma_{\text{jet}} \text{BR}}{k_N F_{\text{jet}}} + \left( \frac{\sigma_{\text{jet}}}{F_{\text{jet}}} \right)^3 \right)^2 - \left( \frac{\sigma_{\text{jet}}}{F_{\text{jet}}} \right)^6} \right\}^{1/3} + \frac{\sigma_{\text{jet}}}{F_{\text{jet}}}. \end{aligned} \quad (38)$$

$\lambda^2$  is easily obtained from Eqs. (35) and (38),

TABLE IV. Numerical value of  $k_N$  for a target nucleus  $N$  in each case.

	C	Al	Si	Ti	Au
case I	$13.83 \left( \frac{1\text{TeV}}{m_{\bar{\nu}_\tau}} \right)^4$	$20.92 \left( \frac{1\text{TeV}}{m_{\bar{\nu}_\tau}} \right)^4$	$20.80 \left( \frac{1\text{TeV}}{m_{\bar{\nu}_\tau}} \right)^4$	$35.71 \left( \frac{1\text{TeV}}{m_{\bar{\nu}_\tau}} \right)^4$	$26.26 \left( \frac{1\text{TeV}}{m_{\bar{\nu}_\tau}} \right)^4$
case II	$3.913 \left( \frac{1\text{TeV}}{m_{\bar{\nu}_\tau}} \right)^4$	$5.881 \left( \frac{1\text{TeV}}{m_{\bar{\nu}_\tau}} \right)^4$	$5.886 \left( \frac{1\text{TeV}}{m_{\bar{\nu}_\tau}} \right)^4$	$9.962 \left( \frac{1\text{TeV}}{m_{\bar{\nu}_\tau}} \right)^4$	$7.185 \left( \frac{1\text{TeV}}{m_{\bar{\nu}_\tau}} \right)^4$
case III	$32.46 \left( \frac{1\text{TeV}}{m_{\bar{\nu}_\tau}} \right)^4$	$48.97 \left( \frac{1\text{TeV}}{m_{\bar{\nu}_\tau}} \right)^4$	$48.83 \left( \frac{1\text{TeV}}{m_{\bar{\nu}_\tau}} \right)^4$	$83.38 \left( \frac{1\text{TeV}}{m_{\bar{\nu}_\tau}} \right)^4$	$60.91 \left( \frac{1\text{TeV}}{m_{\bar{\nu}_\tau}} \right)^4$

$$\lambda^2 = \frac{\text{BR}}{k_N \lambda_{311}^2} = \frac{\text{BR}}{k_N} \left\{ \frac{\sigma_{\text{jet}}}{F_{\text{jet}}} + \left[ \left( \frac{2\sigma_{\text{jet}}\text{BR}}{k_N F_{\text{jet}}} \right) + \left( \frac{\sigma_{\text{jet}}}{F_{\text{jet}}} \right)^3 + \sqrt{\left( \frac{2\sigma_{\text{jet}}\text{BR}}{k_N F_{\text{jet}}} + \left( \frac{\sigma_{\text{jet}}}{F_{\text{jet}}} \right)^3 \right)^2 - \left( \frac{\sigma_{\text{jet}}}{F_{\text{jet}}} \right)^6} \right]^{1/3} \right. \\ \left. + \left[ \left( \frac{2\sigma_{\text{jet}}\text{BR}}{k_N F_{\text{jet}}} \right) + \left( \frac{\sigma_{\text{jet}}}{F_{\text{jet}}} \right)^3 - \sqrt{\left( \frac{2\sigma_{\text{jet}}\text{BR}}{k_N F_{\text{jet}}} + \left( \frac{\sigma_{\text{jet}}}{F_{\text{jet}}} \right)^3 \right)^2 - \left( \frac{\sigma_{\text{jet}}}{F_{\text{jet}}} \right)^6} \right]^{1/3} \right\}^{-1}. \quad (39)$$

As a result, by substituting  $\lambda_{311}^2$  and  $\lambda^2$  into the expression of  $\sigma(pp \rightarrow \mu^- e^+)$  [Eq. (25)], we obtain the prediction of  $\sigma(pp \rightarrow \mu^- e^+)$  as a function of BR and  $\sigma_{\text{jet}}$ ,

$$\sigma(pp \rightarrow \mu^- e^+) = \frac{12}{16\pi} F_{d\bar{d}} m_{\bar{\nu}_\tau} \frac{(\text{BR}/k_N)}{3\lambda_{311}^2 + 8\lambda^2}. \quad (40)$$

Once  $\sigma_{\text{jet}}$  is measured, we can evaluate  $\sigma(pp \rightarrow \mu^- e^+)$  as a function of BR with Eq. (40). Note that the solution, Eqs. (38) and (39), is uniquely determined as read in Fig. 4, and hence  $\sigma(pp \rightarrow \mu^- e^+)$  is also uniquely inferred. We cannot, however, determine  $\sigma_{\text{jet}}$  uniquely

from BR and  $\sigma(pp \rightarrow \mu^- e^+)$  since as a function of BR the latter is a two-valued function as is shown in Fig. 4. Therefore, there are crosses of two lines in Figs. 5 and 6.

We quantitatively analyze the behavior for two reference points. As a first reference point, we take  $N = \text{Al}$ ,  $m_{\bar{\nu}_\tau} = 1 \text{ TeV}$ ,  $\sqrt{s} = 100 \text{ TeV}$ , and  $\sigma_{\text{jet}} = 1 \text{ fb}$ . In this point, when  $\text{BR} \lesssim 10^{-13}$ ,  $\lambda_{311}^2$  and  $\lambda^2$  are approximately calculated from Eqs. (38) and (39) as follows:

$$\lambda_{311}^2 \approx 3 \left( \frac{\sigma_{\text{jet}}}{F_{\text{jet}}} \right), \quad \lambda^2 = \frac{\text{BR}}{k_{\text{Al}} \lambda_{311}^2} = \frac{\text{BR}}{3k_{\text{Al}}} \left( \frac{F_{\text{jet}}}{\sigma_{\text{jet}}} \right). \quad (41)$$

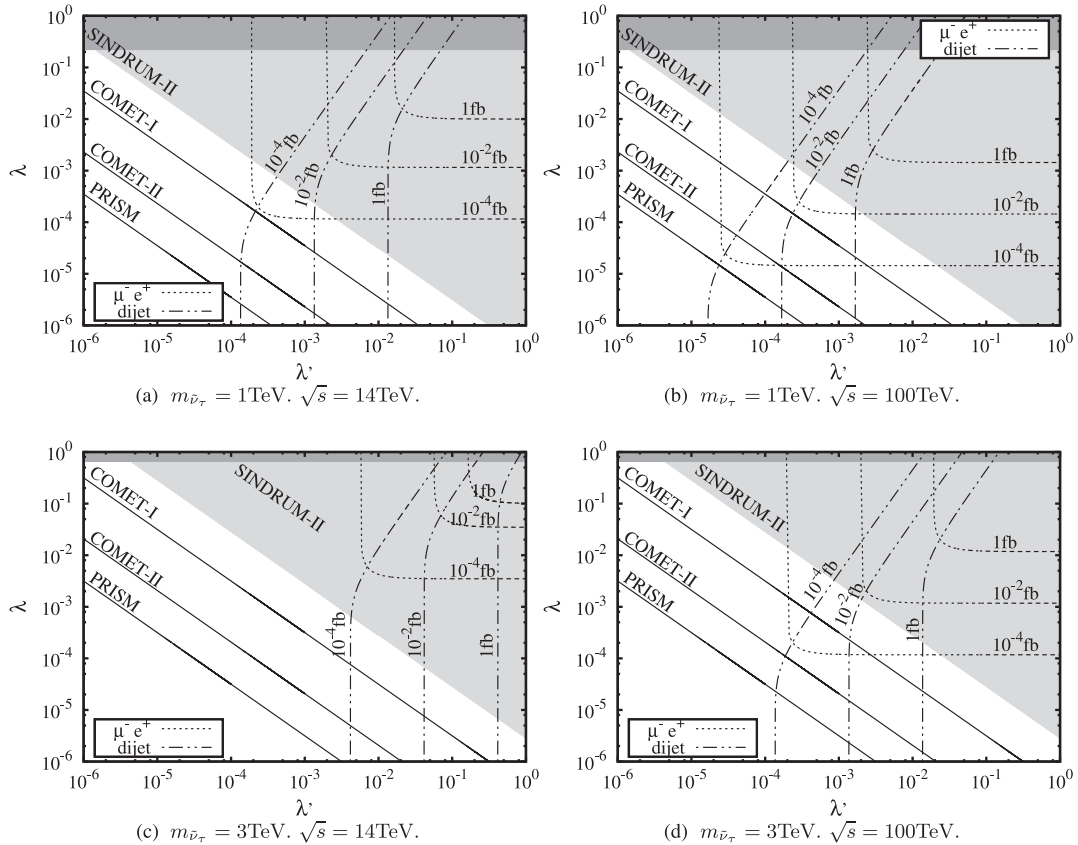


FIG. 7. Contour plot of  $\sigma(pp \rightarrow \mu^- e^+)$ ,  $\sigma(pp \rightarrow jj)$ , and  $\text{BR}(\mu^- N \rightarrow e^- N)$  in case II for (a)  $m_{\bar{\nu}_\tau} = 1 \text{ TeV}$  and  $\sqrt{s} = 14 \text{ TeV}$ , (b)  $m_{\bar{\nu}_\tau} = 1 \text{ TeV}$  and  $\sqrt{s} = 100 \text{ TeV}$  (c)  $m_{\bar{\nu}_\tau} = 3 \text{ TeV}$  and  $\sqrt{s} = 14 \text{ TeV}$  (d)  $m_{\bar{\nu}_\tau} = 3 \text{ TeV}$  and  $\sqrt{s} = 100 \text{ TeV}$ . For simplicity, we take universal RPV coupling,  $\lambda \equiv \lambda_{312} = \lambda_{321} = -\lambda_{132} = -\lambda_{231}$ . Light shaded region is excluded by the  $\mu$ - $e$  conversion search [4], and dark shaded band is excluded region by the  $M$ - $\bar{M}$  conversion search [40].

By substituting  $\lambda'_{311}$  and  $\lambda^2$  into Eq. (25), we obtain the approximate expression of  $\sigma(pp \rightarrow \mu^- e^+)$  and find the BR dependence on  $\sigma(pp \rightarrow \mu^- e^+)$  as follows:

$$\begin{aligned} \sigma(pp \rightarrow \mu^- e^+) &\simeq \frac{12}{16\pi} F_{d\bar{d}m_{\bar{\nu}_\tau}} \frac{\text{BR}/k_{\text{Al}}}{3 \cdot 3 \left(\frac{\sigma_{\text{jet}}}{F_{\text{jet}}}\right) + 8 \cdot \frac{\text{BR}}{3k_{\text{Al}}} \left(\frac{F_{\text{jet}}}{\sigma_{\text{jet}}}\right)} \\ &\simeq \frac{1}{12\pi} F_{d\bar{d}m_{\bar{\nu}_\tau}} \left(\frac{F_{\text{jet}}}{\sigma_{\text{jet}} k_{\text{Al}}}\right) \text{BR}. \end{aligned} \quad (42)$$

The BR dependence is consistent with the numerical result in Fig. 6. As a second reference point, we take  $N = \text{Al}$ ,  $m_{\bar{\nu}_\tau} = 1 \text{ TeV}$ ,  $\sqrt{s} = 100 \text{ TeV}$ , and  $\sigma_{\text{jet}} = 10^{-4} \text{ fb}$ . At this point, when  $\text{BR} \gtrsim 10^{-21}$ ,  $\lambda'_{311}$  and  $\lambda^2$  are approximately calculated from Eqs. (38) and (39) as follows:

$$\begin{aligned} \lambda'_{311} &\simeq 4 \left(\frac{\sigma_{\text{jet}} \text{BR}}{k_{\text{Al}} F_{\text{jet}}}\right)^{1/3}, \\ \lambda^2 &= \frac{\text{BR}}{k_{\text{Al}} \lambda'^2_{311}} = \frac{1}{4} \left(\frac{(\text{BR})^2 F_{\text{jet}}}{k_{\text{Al}}^2 \sigma_{\text{jet}}}\right)^{1/3}. \end{aligned} \quad (43)$$

By substituting  $\lambda'_{311}$  and  $\lambda^2$  into Eq. (25), we obtain the approximate expression of  $\sigma(pp \rightarrow \mu^- e^+)$  and find the BR dependence on  $\sigma(pp \rightarrow \mu^- e^+)$  as follows:

$$\begin{aligned} \sigma(pp \rightarrow \mu^- e^+) &\simeq \frac{12}{16\pi} F_{d\bar{d}m_{\bar{\nu}_\tau}} \\ &\quad \times \frac{\text{BR}/k_{\text{Al}}}{3 \cdot 4 \left(\frac{\sigma_{\text{jet}} \text{BR}}{k_{\text{Al}} F_{\text{jet}}}\right)^{1/3} + 8 \cdot \frac{1}{4} \left(\frac{(\text{BR})^2 F_{\text{jet}}}{k_{\text{Al}}^2 \sigma_{\text{jet}}}\right)^{1/3}} \\ &\simeq \frac{3}{8\pi} F_{d\bar{d}m_{\bar{\nu}_\tau}} \left(\frac{\sigma_{\text{jet}}}{k_{\text{Al}} F_{\text{jet}}}\right)^{1/3} (\text{BR})^{1/3}. \end{aligned} \quad (44)$$

The BR dependence is consistent with the numerical result in Fig. 6. Also, on other points, we can similarly check the BR dependence and find its consistency.

In Figs. 5 and 6, in some regions of  $\text{BR}(\mu^- N \rightarrow e^- N)$ , larger  $\sigma(pp \rightarrow jj)$  suggests smaller  $\sigma(pp \rightarrow \mu^- e^+)$ . This strange relation is simply understood as follows. Large  $\sigma(pp \rightarrow jj)$  for a fixed  $\text{BR}(\mu^- N \rightarrow e^- N)$  leads to large  $\lambda'_{311}$  and small  $\lambda$  [see Eqs. (15) and (26)]. In this case, as is shown in Eq. (40),  $\sigma(pp \rightarrow \mu^- e^+) \propto 1/\lambda'^2_{311}$ . Thus, in

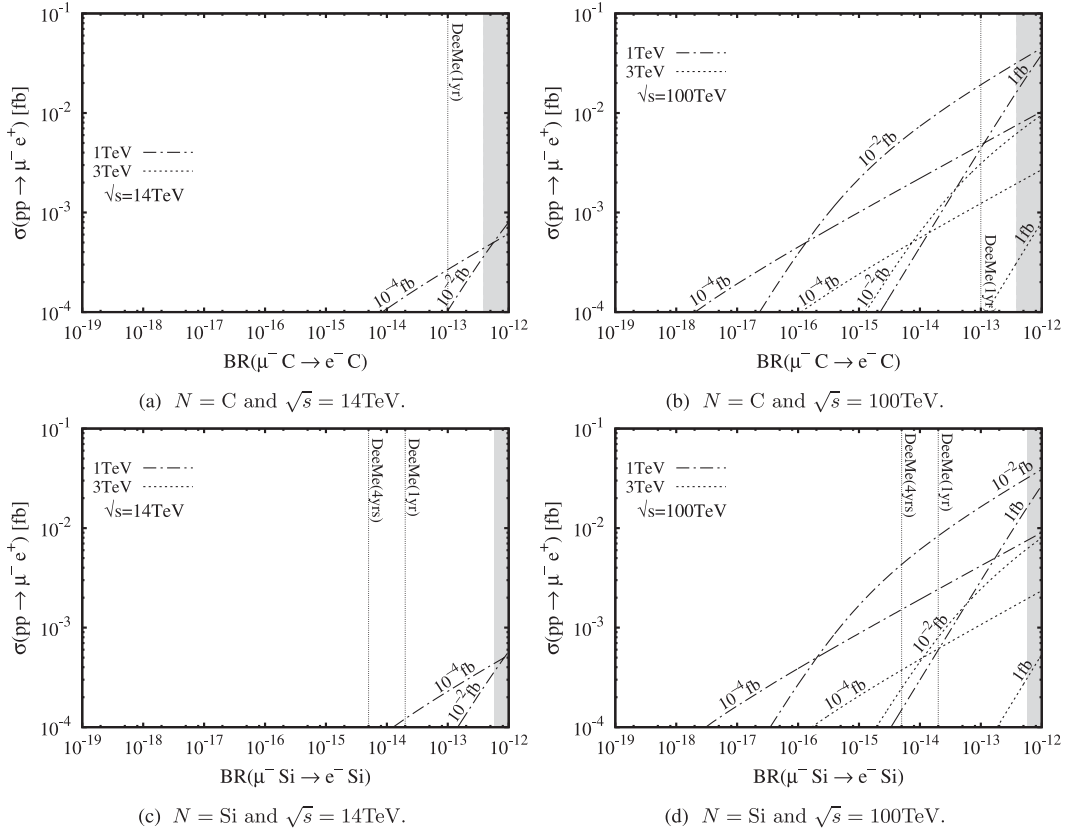


FIG. 8.  $\sigma(pp \rightarrow \mu^- e^+)$  as a function of  $\text{BR}(\mu^- N \rightarrow e^- N)$  for each  $\sigma(pp \rightarrow jj)$  in case II.  $\sigma(pp \rightarrow jj)$  are attached on each line. Results for  $m_{\bar{\nu}_\tau} = 1 \text{ TeV}$  ( $m_{\bar{\nu}_\tau} = 3 \text{ TeV}$ ) are given by the dot-dashed line (dotted line). Shaded regions are the excluded region by the SINDRUM-II experiment. Left panels show the results for the collision energy  $\sqrt{s} = 14 \text{ TeV}$ , and right panels show the results for  $\sqrt{s} = 100 \text{ TeV}$ . We take C [(a) and (b)], and Si [(c) and (d)] for the target nucleus of the  $\mu$ - $e$  conversion process.

some regions, we find the strange relation. This is one of the unique relations in the RPV scenario. In other models, if the mediator universally couples to both quarks and leptons, we will not find the difference between  $\sigma(pp \rightarrow jj)$  and  $\sigma(pp \rightarrow \mu^- e^+)$  (except for color factor). We can distinguish such models from the RPV scenarios by checking the unique relation.

### B. Case II ( $\lambda'_{311} = 0$ and $\lambda'_{322} \neq 0$ )

Figure 7 displays the parameter dependence of  $\sigma(pp \rightarrow \mu^- e^+)$ ,  $\sigma(pp \rightarrow jj)$ , and  $\text{BR}(\mu^- \text{Al} \rightarrow e^- \text{Al})$  in case II. The description of Fig. 7 is the same as that of Fig. 4. Figures 8 and 9 show  $\sigma(pp \rightarrow \mu^- e^+)$  as a function of  $\text{BR}(\mu^- \text{Al} \rightarrow e^- \text{Al})$  in case II. The descriptions of the figures are same as those of Figs. 5 and 6.

The RPV parameters are determined by measuring  $\sigma(pp \rightarrow \mu^- e^+)$ ,  $\sigma(pp \rightarrow jj)$ , and  $\text{BR}(\mu^- \text{Al} \rightarrow e^- \text{Al})$ , and plotting the point on Fig. 7. Since  $\sigma(pp \rightarrow \mu^- e^+)$  at 14 TeV LHC is too small for the parameter determination, we must focus on the invariant mass from the dijet. Precise measurements both of the tau sneutrino mass and  $\sigma(pp \rightarrow jj)$  specify a contour of  $\sigma(pp \rightarrow jj)$  in the  $\lambda'_{322}$ - $\lambda$  plane.

Then the precise measurement of  $\text{BR}(\mu^- \text{Al} \rightarrow e^- \text{Al})$  can pin down the right parameter set on the contour. The accuracy of the pin-down strongly depends on the accuracy both of the invariant mass reconstruction and measurement of  $\text{BR}(\mu^- \text{Al} \rightarrow e^- \text{Al})$ . We will discuss the issue in detail in a separate publication [42].

After the discovery of the  $\mu$ - $e$  conversion signal, if the constructed invariant mass is heavier than 1 TeV in measuring  $pp \rightarrow \mu^- e^+$  and  $pp \rightarrow jj$  at  $\sqrt{s} = 14$  TeV, case II is ruled out. In case II, the accessible parameter space at the LHC with the  $\sqrt{s} = 14$  TeV collision is limited to within the space for lighter tau sneutrino,  $m_{\tilde{\nu}_\tau} \lesssim 1$  TeV. This is because both  $\sigma(pp \rightarrow \mu^- e^+)$  and  $\sigma(pp \rightarrow jj)$  are too small due to the low density of the strange quark component in a proton (see Fig. 3). We need the 100 TeV hadron collider to explore the parameter space for heavier sneutrino,  $m_{\tilde{\nu}_\tau} \gtrsim 1$  TeV, in case II.

Because of the low density of the strange quark component in a proton, the reaction rate of the  $\mu$ - $e$  conversion in case II is clearly different from that in cases I and III. For a fixed combination of  $\sigma(pp \rightarrow \mu^- e^+)$  and  $\sigma(pp \rightarrow jj)$ , the expected  $\text{BR}(\mu^- N \rightarrow e^- N)$  is small compared with that in cases I and III [Eqs. (17)–(20)], and hence it is easy to

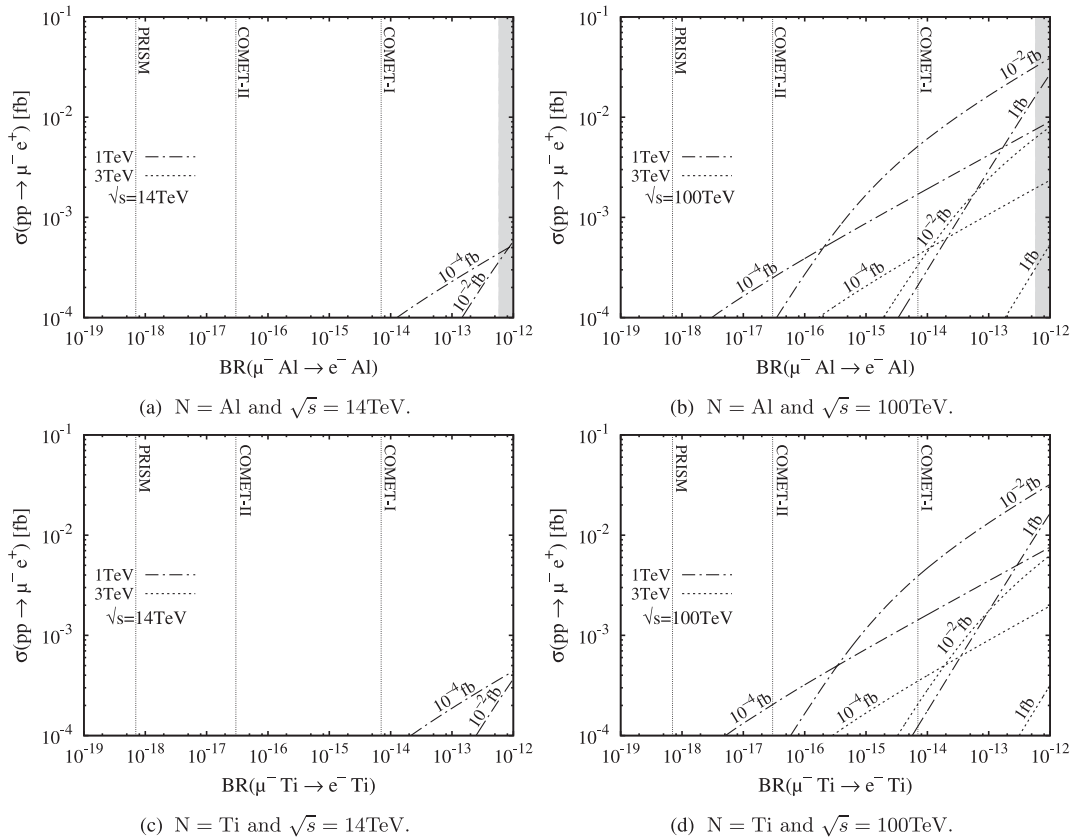


FIG. 9. Same as Fig. 8 except for the target nucleus. We take Al [(a) and (b)] and Ti [(c) and (d)] for the target nucleus of the  $\mu$ - $e$  conversion process.

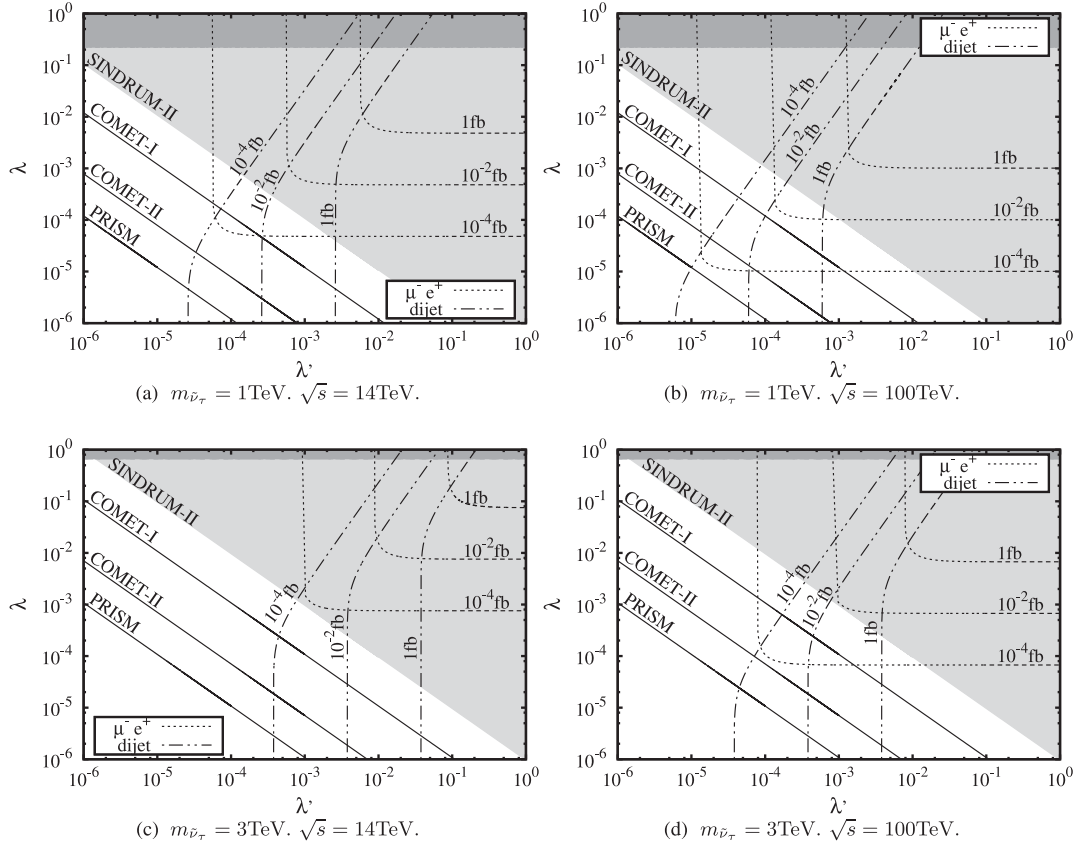


FIG. 10. Contour plot of  $\sigma(pp \rightarrow \mu^- e^+)$ ,  $\sigma(pp \rightarrow jj)$ , and  $\text{BR}(\mu^- N \rightarrow e^- N)$  in case III for (a)  $m_{\tilde{\nu}_\tau} = 1$  TeV and  $\sqrt{s} = 14$  TeV, (b)  $m_{\tilde{\nu}_\tau} = 1$  TeV and  $\sqrt{s} = 100$  TeV, (c)  $m_{\tilde{\nu}_\tau} = 3$  TeV and  $\sqrt{s} = 14$  TeV, (d)  $m_{\tilde{\nu}_\tau} = 3$  TeV and  $\sqrt{s} = 100$  TeV. For simplicity, we take the universal RPV coupling,  $\lambda \equiv \lambda_{312} = \lambda_{321} = -\lambda_{132} = -\lambda_{231}$ . The light-shaded region is excluded by the  $\mu$ - $e$  conversion search [4], and the dark-shaded band is the region excluded by the  $M$ - $\bar{M}$  conversion search [40].

discriminate the case-II scenario from cases I and III by checking the correlations in Figs. 8 and 9. It is important to emphasize that we have to exhibit the correlations in order to verify the RPV scenarios where cLFV processes are never found, except for  $\mu$ - $e$  conversion. It is the first time that these correlations have been graphically shown in RPV SUSY models.

### C. Case III ( $\lambda'_{311} \neq 0$ and $\lambda'_{322} \neq 0$ )

Figure 10 displays the parameter dependence of  $\sigma(pp \rightarrow \mu^- e^+)$ ,  $\sigma(pp \rightarrow jj)$ , and  $\text{BR}(\mu^- \text{Al} \rightarrow e^- \text{Al})$  in case III. The description of Fig. 10 is the same as that of Fig. 4. Figures 11 and 12 show  $\sigma(pp \rightarrow \mu^- e^+)$  as a function of  $\text{BR}(\mu^- \text{Al} \rightarrow e^- \text{Al})$  in case III. The description of the figure is the same as those in Figs. 5 and 6.

We can check the nice consistency between theoretical calculations and the behavior of plots in Figs. 11 and 12 by repeating the same quantitative analysis in Sec. IV A with  $F_{\text{jet}}$  and  $k_N$  for case III (see Table IV).

We can discriminate cases I, II, and III from one another by checking the correlations of  $\sigma(pp \rightarrow \mu^- e^+)$ ,  $\sigma(pp \rightarrow jj)$ , and  $\text{BR}(\mu^- \text{Al} \rightarrow e^- \text{Al})$  with Figs. 5, 6, 8, 9, 11, and 12. And, as we discussed in cases I and II, the RPV couplings are precisely determined via the measurement  $\sigma(pp \rightarrow \mu^- e^+)$ ,  $\sigma(pp \rightarrow jj)$ , and  $\text{BR}(\mu^- \text{Al} \rightarrow e^- \text{Al})$  by using Fig. 10.

### D. Comment for NSI

In Figs. 10, 11, and 12, for simplicity, we take  $\lambda'_{311} = \lambda'_{322}$ . When we take  $\lambda'_{311} \neq \lambda'_{322}$ , as is studied in Sec. III A and Sec. III B, behavior of the plots is basically the same as in Figs. 10, 11, and 12. In such a case, in order to determine  $\lambda'_{311}$  and  $\lambda'_{322}$  separately, we need another measurement, say that of the NSI at next-generation neutrino experiments.

It is said that  $\epsilon_{\mu e}^S$  of ( $10^{-4}$ ) can be searched in the near future [43]. However, from the current limit of the branching ratio of the  $\mu \rightarrow e$  conversion, it must be less than  $10^{-6}$  which is far below the expected sensitivity.

We leave the detailed study for future work [42].

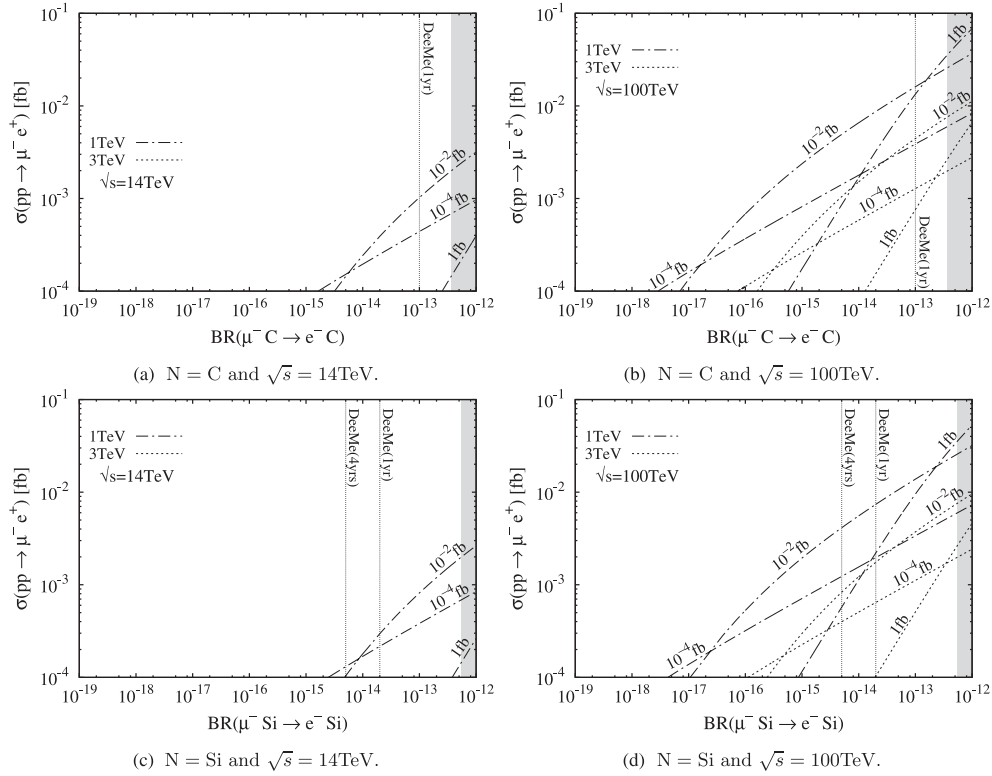


FIG. 11.  $\sigma(pp \rightarrow \mu^- e^+)$  as a function of  $\text{BR}(\mu^- N \rightarrow e^- N)$  for each  $\sigma(pp \rightarrow jj)$  in case III.  $\sigma(pp \rightarrow jj)$  are attached on each line. Results for  $m_{\tilde{\nu}_e} = 1\text{ TeV}$  ( $m_{\tilde{\nu}_e} = 3\text{ TeV}$ ) are given by the dot-dashed line (dotted line). The shaded region in each panel is the region excluded by the SINDRUM-II experiment. Left panels show the results for the collision energy  $\sqrt{s} = 14\text{ TeV}$ , and right panels show the results for  $\sqrt{s} = 100\text{ TeV}$ . We take C [(a) and (b)] and Si [(c) and (d)] for the target nucleus of the  $\mu$ - $e$  conversion process.

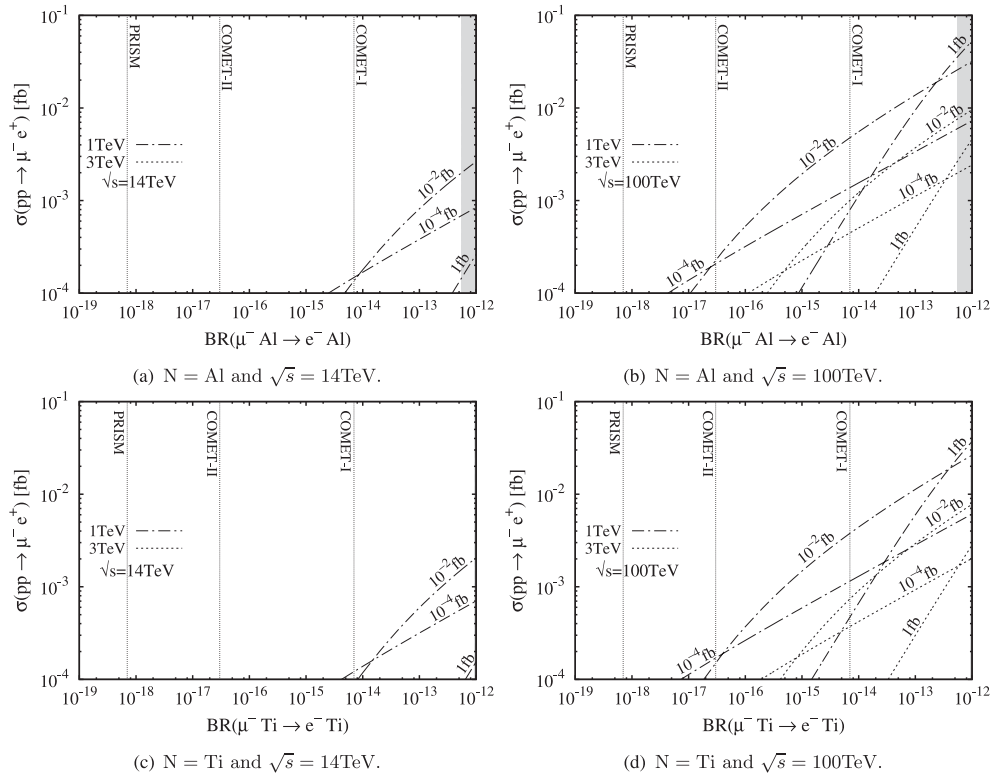


FIG. 12. Same as Fig. 11 except for the target nucleus. We take Al [(a) and (b)] and Ti [(c) and (d)] for the target nucleus of the  $\mu$ - $e$  conversion process.

## V. SUMMARY AND DISCUSSION

The COMET and DeeMe experiments will launch soon and search for the  $\mu$ - $e$  conversion signal. This work supposes the case where the  $\mu$ - $e$  conversion is discovered while other cLFV muon decays are never found. We sorted out expected interactions realized in such a case and discussed the approaches to confirm the  $\mu$ - $e$  conversion signal without conventional cLFV searches.

We have studied a supersymmetric standard model without  $R$  parity as a benchmark case, where COMET and DeeMe observe  $\mu$ - $e$  conversion prior to all the other experiments observing new physics. In this case, with the assumption that only the third-generation sleptons contribute to such a process, we need to assume that  $\{\lambda'_{311}$  and/or  $\lambda'_{322}\} \times \{\lambda_{312}$  and/or  $\lambda_{321}\}$  must be sufficiently large. Though other combinations of coupling constants can lead to a significant  $\mu$ - $e$  conversion process, only those are considered here. This is because in most of scenarios in the supersymmetric theory, the third generation of the scalar lepton has the lightest mass.

With these assumptions, we calculated the effects on future experiments. First, we considered the sensitivity of the future  $\mu$ - $e$  conversion experiments on the couplings and the masses. To do this we considered three cases: (I)  $\lambda'_{311}$  is dominant, (II)  $\lambda'_{322}$  is dominant, and (III) both are dominant. Since the matrix element of  $\bar{q}q$  in the nucleus is different for the down quark and strange quark, we found a different sensitivity with them.

Then with the sensitivity kept in mind, we estimated the reach to the couplings by calculating the cross section of  $pp \rightarrow \mu^- e^+$  and  $pp \rightarrow jj$  as a function of the slepton masses and the couplings. To have a signal of  $\mu^- e^+$ , both the coupling  $\lambda'$  and  $\lambda$  must be large and, hence, there are

lower bounds for them. To observe the dijet event via the slepton, however, only the coupling  $\lambda'$  must be large and, hence, there is a lower bound on it (Figs. 4, 7, and 10). In all cases we have a chance to get confirmation of the  $\mu$ - $e$  conversion in the LHC indirectly. In addition, we put a bound on the couplings by comparing both modes.

Contrary to the hope with the LHC, unfortunately, the current bound by the  $\mu$ - $e$  conversion gives the much smaller rate of the nonstandard interaction than the sensitivity in near future experiments. Nonetheless the small rate, the nonstandard interaction makes it possible to distinguish  $\lambda_{312}$  and  $\lambda_{321}$ , and hence it is worth searching for it.

Finally, we considered muonium conversion. If  $\lambda'$  is very small, we cannot expect a signal from LHC. In this case, at least one of  $\lambda_{312}$  and  $\lambda_{321}$  must be very large. With a little luck, both of them are very large and we can expect muonium conversion.

There are other opportunities to check the result of  $\mu$ - $e$  conversion. For example, we can distinguish  $\lambda_{312}$  and  $\lambda_{321}$  in the linear collider with a polarized beam. We can also expect the signal  $pe^- \rightarrow p\mu^-$  in the LHeC. Furthermore, the improvement of the calculation of the  $\mu$ - $e$  conversion rate is important to determine the model parameters [44]. It is, however, beyond the scope of this paper to estimate their sensitivities and to improve the calculation. We leave them for a future work [42].

## ACKNOWLEDGMENTS

This work was supported in part by the Grants-in-Aid for the Ministry of Education, Culture, Sports, Science, and Technology, Government of Japan, No. 24340044 and No. 25105009 (J. S.) and No. 25003345 (M. Y.).

- 
- [1] Y. Kuno and Y. Okada, *Rev. Mod. Phys.* **73**, 151 (2001).
  - [2] M. L. Brooks *et al.* (MEGA Collaboration), *Phys. Rev. Lett.* **83**, 1521 (1999).
  - [3] J. Adam *et al.* (MEG Collaboration), *Phys. Rev. Lett.* **110**, 201801 (2013).
  - [4] W. H. Bertl *et al.* (SINDRUM II Collaboration), *Eur. Phys. J. C* **47**, 337 (2006).
  - [5] U. Bellgardt *et al.* (SINDRUM Collaboration), *Nucl. Phys.* **B299**, 1 (1988).
  - [6] B. Aubert *et al.* (BABAR Collaboration), *Phys. Rev. Lett.* **92**, 121801 (2004).
  - [7] K. Abe *et al.* (Belle Collaboration), *Phys. Rev. Lett.* **92**, 171802 (2004).
  - [8] K. Hayasaka *et al.* (Belle Collaboration), *Phys. Lett. B* **613**, 20 (2005).
  - [9] Y. Enari *et al.* (Belle Collaboration), *Phys. Lett. B* **622**, 218 (2005).
  - [10] Y. Fukuda *et al.* (Super-Kamiokande Collaboration), *Phys. Rev. Lett.* **81**, 1562 (1998).
  - [11] K. Abe *et al.* (T2K Collaboration), *Phys. Rev. Lett.* **112**, 061802 (2014).
  - [12] R. Aaij *et al.* (LHCb Collaboration), *Phys. Lett. B* **724**, 36 (2013).
  - [13] Y. G. Cui *et al.* (COMET Collaboration), Report No. KEK-2009-10.
  - [14] Y. Kuno (COMET Collaboration), *PTEP* **2013**, 022C01 (2013).
  - [15] H. Natori (DeeMe Collaboration), *Nucl. Phys. B Proc. Suppl.* **248–250**, 52 (2014).
  - [16] J. Hisano, T. Moroi, K. Tobe, and M. Yamaguchi, *Phys. Rev. D* **53**, 2442 (1996).
  - [17] J. Sato and K. Tobe, *Phys. Rev. D* **63**, 116010 (2001).
  - [18] A. de Gouvea, S. Lola, and K. Tobe, *Phys. Rev. D* **63**, 035004 (2001).

- [19] K. Huitu, J. Maalampi, M. Raidal, and A. Santamaria, *Phys. Lett. B* **430**, 355 (1998).
- [20] T. S. Kosmas, S. Kovalenko, and I. Schmidt, *Phys. Lett. B* **519**, 78 (2001).
- [21] M. Frank and K. Huitu, *Phys. Rev. D* **64**, 095015 (2001).
- [22] H. K. Dreiner, K. Nickel, F. Staub, and A. Vicente, *Phys. Rev. D* **86**, 015003 (2012).
- [23] K. Huitu and H. Waltari, *J. High Energy Phys.* **11** (2014) 053.
- [24] D. N. Dinh, A. Ibarra, E. Molinaro, and S. T. Petcov, *J. High Energy Phys.* **08** (2012) 125; **09** (2013) 23.
- [25] R. Alonso, M. Dhen, M. B. Gavela, and T. Hambye, *J. High Energy Phys.* **01** (2013) 118.
- [26] T. Toma and A. Vicente, *J. High Energy Phys.* **01** (2014) 160.
- [27] A. Abada, M. E. Krauss, W. Porod, F. Staub, A. Vicente, and C. Weiland, *J. High Energy Phys.* **11** (2014) 048.
- [28] M. Koike, Y. Kuno, J. Sato, and M. Yamanaka, *Phys. Rev. Lett.* **105**, 121601 (2010).
- [29] S. Weinberg, *Phys. Rev. D* **26**, 287 (1982).
- [30] N. Sakai and T. Yanagida, *Nucl. Phys.* **B197**, 533 (1982).
- [31] L. J. Hall and M. Suzuki, *Nucl. Phys.* **B231**, 419 (1984).
- [32] J. E. Kim, P. Ko, and D.-G. Lee, *Phys. Rev. D* **56**, 100 (1997).
- [33] R. Kitano, M. Koike, and Y. Okada, *Phys. Rev. D* **66**, 096002 (2002); **76**, 059902(E) (2007).
- [34] T. S. Kosmas, S. Kovalenko, and I. Schmidt, *Phys. Lett. B* **511**, 203 (2001).
- [35] J. Pumplin, D. R. Stump, J. Huston, H. L. Lai, P. M. Nadolsky, and W. K. Tung, *J. High Energy Phys.* **07** (2002) 012.
- [36] A. I. Vaĭnshteĭn, V. I. Zakharov, and M. A. Schifman, *Pis'ma Zh. Eksp. Teor. Fiz.* **22**, 123 (1975) [*JETP* **22**, 55 (1975)].
- [37] T. Ota and J. Sato, *Phys. Lett. B* **545**, 367 (2002).
- [38] T. Ota, J. Sato, and N.-a. Yamashita, *Phys. Rev. D* **65**, 093015 (2002).
- [39] K. Horikawa and K. Sasaki, *Phys. Rev. D* **53**, 560 (1996).
- [40] L. Willmann, P. V. Schmidt, H. P. Wirtz, R. Abela, V. Baranov, J. Bagaturia, W. H. Bertl, and R. Engfer *et al.*, *Phys. Rev. Lett.* **82**, 49 (1999).
- [41] Mu2e Collaboration, Proposal to search for  $\mu^- + N \rightarrow e^- N$  with a single-event sensitivity below  $10^{-16}$  (Mu2e experiment) (2008), <http://mu2e-docdb.fnal.gov/cgi-bin/ShowDocument?docid=388>.
- [42] J. Sato and M. Yamanaka (to be published).
- [43] J. Kopp, M. Lindner, T. Ota, and J. Sato, *Phys. Rev. D* **77**, 013007 (2008).
- [44] A. Crivellin, M. Hoferichter, and M. Procura, *Phys. Rev. D* **89**, 093024 (2014).